Amplified upward trend of the joint occurrences of heat and ozone extremes in China over 2013–2020

Xiang Xiao,[a] Yangyang Xu,[b] Xiaorui Zhang,[a] Fan Wang,[a] Xiao Lu,[c] Zongwei Cai,[d] Guy Brasseur,[e] Meng Gao[*,a,d,f]

[a] *Department of Geography, Hong Kong Baptist University, Hong Kong, China*

[b] *Department of Atmospheric Sciences, Texas A&M University, College Station, TX, USA*

[c] *School of Atmospheric Sciences, Sun Yat-sen University, Guangzhou, China*

[d] *State Key Laboratory of Environmental and Biological Analysis, Hong Kong Baptist University, Hong Kong, China*

[e] *Atmospheric Chemistry Observation & Modeling Laboratory, National Center for Atmospheric Research, Boulder, CO, USA*

[f] *Hong Kong Branch of Southern Marine Science and Engineering Guangdong Laboratory (Guangzhou), Hong Kong, China*

[*] *Corresponding author: Meng Gao, mmgao2@hkbu.edu.hk*

ABSTRACT

Climate change and air pollution are two intimately interlinked global concerns. The frequency, intensity and duration of heatwaves are projected to increase globally under future climate change. A growing body of evidence indicates that health risks associated with the joint exposure to heatwaves and air pollution can be greater than that due to individual factors. However, the co-occurrences of heat and air pollution extremes in China remain less explored in the observational records. Here we investigate the spatial pattern and temporal trend of frequency, intensity, and duration of co-occurrences of heat and air pollution extremes using China's nationwide observations of hourly $PM_{2.5}$ and O_3, and the ERA5 reanalysis dataset over 2013–2020. We identify a significant increase in the frequency of co-occurrence of wet-bulb temperature (T_w) and O_3 exceedances (beyond a certain predefined threshold), mainly in the Beijing-Tianjin-Hebei (BTH) region (up by 4.7 days decade^{-1}) and the Yangtze River Delta (YRD). In addition, we find that the increasing rate (compared to the average levels during the study period) of joint exceedance is larger than the rate of T_w and O_3 itself. For example, T_w and O_3 co-extremes increased by 7.0% in BTH, higher than the percentage increase of each at 0.9% and 5.5%, respectively. We identify same amplification for YRD. This ongoing upward trend in the joint occurrence of heat and O_3 extremes should be recognized as an emerging environmental issue in China, given the potentially larger compounding impact to public health.

1. Introduction

Global warming and ambient air pollution are two leading global public health concerns, driven by anthropogenic emissions of greenhouse gases and air pollutants from fossil fuel uses (Pachauri et al. 2014). It was estimated that the increase in global temperature would result in additional 250,000 deaths each year between 2030 and 2050 (Watts et al. 2015), while a recent assessment attributed 4.2 million premature deaths per year to ambient air pollution exposure (Cohen et al. 2017; WHO 2020). Climate change and air pollution are also intimately interlinked (Dean; Green 2018). A warming climate could directly alter meteorological variables, such as temperature, precipitation and wind (Sanderson et al. 2011), and thus further affects physical and chemical processes of air pollution [e.g., Ozone (O_3) and particulate matter ≤ 2.5μm, ($PM_{2.5}$)] over multiple spatiotemporal scales (Ebi; McGregor 2008; Kinney 2008; Xu et al. 2018). Climate change is also likely to indirectly change particulate matter (PM) levels by modulating the natural emission from the occurrences of wildfires and dust storms (Dean; Green 2018).

Compared to the mean conditions of weather and air pollution, extreme weather and air pollution events, despite rare occurrences, can pose greater threats to human health and induce larger devastation to ecosystems and economy (Field et al. 2012; Zhang et al. 2020). More concerning is that extreme air pollution episodes and heatwaves often occur simultaneously because they can be driven by some common meteorological conditions. For example, heatwaves, droughts and peak ozone episodes are usually associated with stagnant high-pressure systems (low precipitation, low wind speeds, sufficient solar radiation, etc.) that tend to accumulate heat and ozone precursors in a certain location. Moreover, complex interactions and feedbacks could happen to exacerbate extreme conditions. For example, high temperature during heatwaves enhances biogenic emissions of volatile organic compounds (BVOCs) to increase production of O_3 and secondary organic aerosols (Karl et al. 2003). Under drought stress, stomatal uptake by plants is inhibited to reduce water loss, leading to a weaker dry deposition of O_3 and thus its higher surface concentrations (Gerosa et al. 2009; Lin et al. 2020).

Given that heat waves (Beniston 2004; Meehl and Tebaldi 2004; Stott et al. 2004; Fischer et al. 2007; Cowan et al. 2014; Schär 2016; Hoegh-Guldberg et al. 2018) and air pollution episodes (Mickley et al. 2004; Tagaris et al. 2007; Wu et al. 2008; Gao et al. 2013; Rieder et al. 2015; Schnell et al. 2016; Doherty et al. 2017; Schnell and Prather 2017; Chen et al. 2019) may aggravate over the coming decades, it is of great significance to analyze the historical trends of co-occurrence of heatwave and air pollution extremes, which would shed lights on the fidelity of their future projections. Another imperative to understand the co-occurrence of heatwave and air pollution extremes is driven by the recognitions that the simultaneous exposure to both air pollution and heatwave may amplify the health consequences beyond the sum of individual effects (Basu 2009; Dear et al. 2005; Kan et al. 2012; Li et al. 2014; Ren et al. 2008; Stafoggia et al. 2008; Wang et al. 2020a; Willers et al. 2016; Zanobetti; Peters 2015).

Over the recent decade, air pollution, particularly the high $PM_{2.5}$ levels, have raised wide concerns in China (Gao et al. 2020a; Gao et al. 2020b; Liang et al. 2017), and the State Council of China announced its strictest plan, the Air Pollution Prevention and Control Plan, in September 2013 (Zhang et al. 2019) to reduce the level of air pollutants. Since then, a decreasing trend of $PM_{2.5}$ levels have been found in both satellite and ground-level observations (Lin et al. 2018; Wang et al. 2020b; Wang et al. 2021). Despite of the overall decreasing trend, $PM_{2.5}$ concentrations during some pollution episodes can still exceed the threshold recommended by the World Health Organization (WHO) or local standards adopted in China (Wang et al. 2020b). Notably, while the concentrations of most primary pollutants have been decreasing in response to the emission control plan, surface O_3 concentrations have been increasing in several populated regions of China (Liu; Wang 2020; Lu et al. 2020; Wang et al. 2020b), and is projected to increase (Zhu and Liao, 2016). Nevertheless, the variability and recent trend of the joint frequency of all three detrimental environmental stressors ($PM_{2.5}$, O_3, and heat extremes) have not been extensively explored in China. Here we present a series of spatiotemporal analyses based on various sources of observations from 2013 to 2020 (Section 2). The observationally based results here would be crucial to enhancing environmental protection measures and informing public health policies in the future (Chen et al. 2018; Xu et al. 2020).

2. Methods

2.1 Data Sources of $PM_{2.5}$, O_3 and Temperature

Nationwide observations of hourly $PM_{2.5}$ and O_3 concentrations from year 2013 to 2020 were obtained from the China National Environmental Monitoring Center (CNEMC) network. Starting from 2013 in 74 major cities, the CNEMC network now consists of more than 1600 monitoring sites, covering 367 cities in China. $PM_{2.5}$ and O_3 were reported in unit of $\mu g/m^3$. Daily mean values of $PM_{2.5}$ were calculated from hourly record. Daily maximum 8-hour average (MDA8) of O_3 were calculated as well. Hourly temperature and corresponding dew point temperature were taken from the ERA5 reanalysis dataset by the European Centre for Medium-Range Weather Forecasts (ECMWF) (Hersbach et al. 2020). Both temperature and dew point temperature from ERA5 were sampled at CNEMC sites to examine co-occurrences.

2.2 Definition of heat extremes using Wet-Bulb Temperature

Previous studies suggested that a combination of temperature and humidity is a better metric to assess heat-related health risks (Kovats; Hajat 2008; Mora et al. 2017; Xu et al. 2020) , as human body is less able to cool itself efficiently by sweating under high humidity conditions. We adopted wet-bulb temperature (T_w) in this study as the metric to define occurrences of heatwaves (Sherwood 2018). The calculation of T_w assumes light wind speed and moderate radiation (Knutson; Ploshay 2016; Willett; Sherwood 2012), and thus only accounts for temperature (T) and humidity measures. In this study, we computed T_w using Stull (2011)'s method:

$$T_w = T \cdot \mathrm{atan}\left[0.151977(100 \cdot RH + 8.313659)^{\frac{1}{2}}\right] + \mathrm{atan}(T + 100 \cdot RH) - \mathrm{atan}(100 \cdot RH - 1.676331) + 0.00391838(100 \cdot RH)^{\frac{3}{2}} \cdot \mathrm{atan}(0.023101 \cdot 100 \cdot RH) - 4.686035 \quad (1)$$

where T_w denotes the wet-bulb temperature (°C), T the temperature (°C), RH the relative humidity. Because ERA5 provides dew-point temperature only, RH was calculated by the following equation:

$$e_s = e_0 \cdot \exp\left(\frac{L_v}{R_w}\left(\frac{1}{T_0} - \frac{1}{T}\right)\right),\ e_{dew} = e_0 \cdot \exp\left(\frac{L_v}{R_w}\left(\frac{1}{T_0} - \frac{1}{T_{dew}}\right)\right),\ RH = \frac{e_{dew}}{e_s}\frac{p-e_s}{p-e_{dew}} \times$$

100%, (2)

where e_0 represents the reference water vapor pressure (611 Pa), and e_s and e_{dew} signify the water vapor pressure at saturation and at dew point temperature, respectively. T_0 refers to the reference temperature (273 K). T_{dew} denotes the dew point temperature. L_v is the latent heat of water vaporization from liquid to gas (2.5×10^6 J/kg), and R_w represents the specific gas constant for water vapor (461.5 J/kg/K). Following Xu et al. (2020), we adopted daily average $T_w \geq 25$ °C as the threshold for heat extremes.

2.3 Definition of air pollution extremes

We used the air quality standard of China (Zhao et al. 2016) for $PM_{2.5}$ and O_3, namely 75 μg/m^3 and 160 μg/m^3, as the cut-off values of exceedance. The days when daily mean T_w, daily mean $PM_{2.5}$, or MDA8 value for O_3, were higher than corresponding cut-off values, were marked as exceedance days for each metric. The days when two or more metrics exceed thresholds simultaneously were further marked as co-occurring extreme days. The numbers of exceedance days were summarized by months for further trend analyses.

In addition to number of exceedance days (i.e. frequency of extreme events), we also considered the duration and severity of these extremes (Xu et al. 2020). Duration was defined as the number of successive days of extreme events. The severity was defined as the difference between the long-term average and the corresponding levels within the exceedance days only.

2.4 Statistical Method for Trend Analyses

Previous studies have shown that heatwaves and O_3 extremes often occur in warm seasons while $PM_{2.5}$ is typically more severe in cold seasons in China (Jia et al. 2017; Lu et al. 2020; Zheng et al. 2005), we therefore quantify the trend of T_w and O_3 during warm seasons only (six months from April to September), and for $PM_{2.5}$ we quantified the trend across the entire year. For the co-occurrence of T_w, O_3 and $PM_{2.5}$, we also used data during warm seasons. We assess the trends of monthly exceedance frequency (i.e., days per month) for heatwaves, $PM_{2.5}$ and O_3 from 2013 to 2020, explicitly accounting for seasonal cycles and autocorrelation (Chandler; Scott 2011; Lu et al. 2020), as detailed below.

Trend analyses were performed by constructing a generalized linear regression equation with periodic functions accounting for seasonal variation and an autoregression term accounting for autocorrelation within the study period, as follows:

$$y_t = b + kt + \alpha \cos\left(\frac{2\pi M}{C}\right) + \beta \sin\left(\frac{2\pi M}{C}\right) + AR_t, \quad (3)$$

where y_t represents the exceedance frequency for the metrics of T_w, $PM_{2.5}$ and O_3 in month t, t denotes the index of month during the study period of 8 years (ranging from 1 to 48 for T_w and O_3, or 1 to 96 for $PM_{2.5}$ alone), b denotes the intercept, k is the linear trend coefficient, α and β are coefficients of periodic functions, M is the month index in each year (ranging from 1 to 6 for T_w and O_3, or 1 to 12 for $PM_{2.5}$ alone), C is the length of seasonal cycle (6 for T_w and O_3, or 12 for $PM_{2.5}$ itself) and AR_t is the autoregression term for y_t. Non-parametric Mann-Kendall (M-K) test was performed to test the significance of linear trends.

2.5 Pooling to derive Regional Trend

Previous studies showed that the spatial distribution of O_3 concentrations vary greatly across different regions in China (Lu et al. 2018). Beijing-Tianjin-Hebei (BTH) region, Yangtze River Delta (YRD) and Pearl River Delta (PRD) region are three major urban clusters with distinct pollution patterns (Liu et al. 2018; Ma et al. 2019). In this study, we calculated the aggregated/pooled trend of exceedances for T_w, O_3 and $PM_{2.5}$ as well as their joint occurrences in these three megacity clusters in China (BTH, YRD and PRD).

However, the methods to generate regional trend in previous studies using observation data from monitoring sites seem arbitrary as each monitoring site may have depicted different and even opposite trends. A synthetical statistical algorithm is thus needed to standardize the calculation of regional trend. Here we propose a pooling method to aggregate the trends calculated from all individual sites within a specific region. The site-specific local trend, notated as k_i in Section 2.4, are then pooled to estimate the average trend (K_r) representing a specific region following the equation of:

$$K_r = \frac{\sum_{i=1}^{n} k_i \cdot w_i}{\sum_{i=1}^{n} w_i}, \quad (4)$$

where n is the number of sites within the region, and w_i is the weighting factor for each site $_i$, defined as follow, similar to meta-analysis (Lipsey; Wilson 2001), where the standard error SE_i represents the uncertainty of estimating k_i

$$w_i = 1/SE_i^2, \qquad (5)$$

K_r is approximately normally distributed (Sánchez-Meca; Marín-Martínez 2010) and its sample variance could be defined as:

$$Var(K_r) = 1/\sum_{i=1}^{n} w_i, \qquad (6)$$

3. Results and Discussion

3.1 Spatiotemporal variations and long-term trend of T_w, O_3 and $PM_{2.5}$ exceedances

Humidity has critical effects on human body's reaction to temperature (Liu et al. 2014) as human body is not able to cool itself by sweating under high humidity. Using temperature only may underestimate the severity of heatwaves, especially in humid regions (Russo et al. 2017). In this study, we adopted 25 °C as the threshold of heat extremes as proposed by Mora et al. (2017), and note that 25 °C at a typical RH of 40% is very close to daily max temperature of 35 °C (Xu et al. 2020). Over the southeastern coastal regions, T_w exceedance days could reach as high as 150–180 days annually (Figure 1a and S1), suggesting high frequency of heatwaves there. The average T_w in China displays a slightly increasing trend, rising from 13.5 °C (standard deviation, SD: 5.6 °C) in 2013 to 13.8 °C (SD: 5.5 °C) in 2020

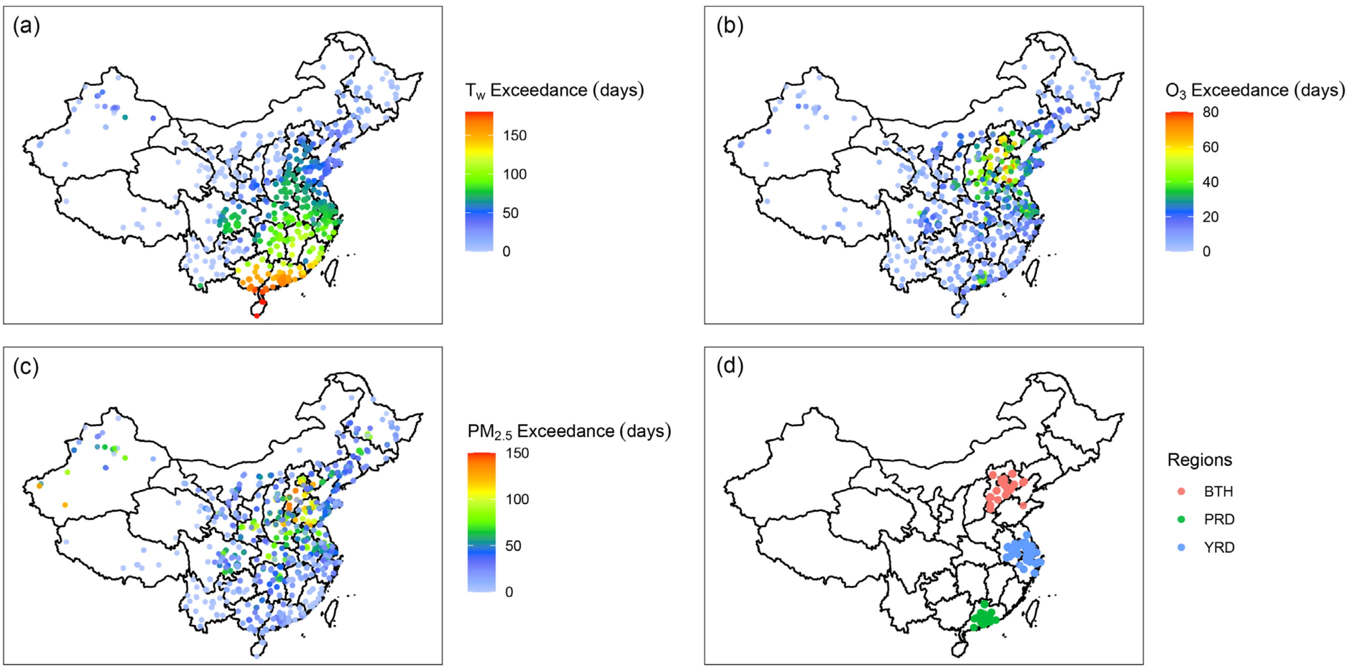

Fig. 1. Average number of exceedance days per year for T_w (a), O_3 (b) and $PM_{2.5}$ (c); locations of the sites in the BTH, PRD and YRD regions (d).

(Figure S2). Moreover, the severity of high T_w extremes could reach up to 3 °C (Figure S3) and the events (mean duration) could last about two months in southernmost part of China (Figure S4). Previously, Ding et al. (2010) and Wei; Chen (2011) reported a significant increase in heatwaves across the nation during recent decades, except for a slight decrease in central China. In the shorter period of the last decade as examined here, however, the trend of T_w exceedance can go in both directions across China (Figure 2). Overall, a clear positive trend could be found in mid-eastern and northeastern regions, on average, at rates of up to 1.4 days decade^{-1}. In contrast, a decreasing trend, around 1.0 days decade^{-1} on average, is found in coastal and central areas of China.

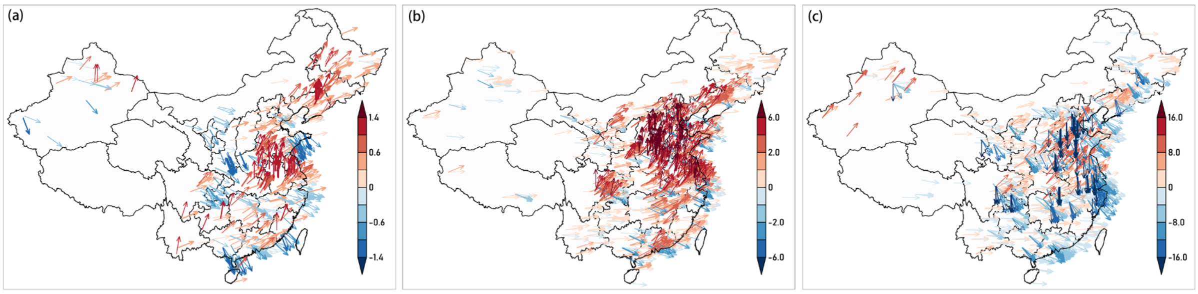

Fig. 2. Trend of T_w (a,), O_3 (b) and $PM_{2.5}$ (c) exceedance days. *Both the angle and color are showing the negative trends (i.e., downward sloping arrows in blue color) and positive trends (i.e., upward sloping arrows in red color)*

Occurrences of O_3 exceedance were concentrated in the BTH, YRD, and PRD (locations marked in Figure 1d), where intense human activities are located (Figure 1b). Exceedance days exhibited a general increase over 2013-2020 (up to 6.0 days decade^{-1}, Figure 2b), in line with the variations of O_3 levels (Figure S5 and S6). Despite that extremely high levels of MDA8 O_3 (i.e., > 30 μg/m^3 above the threshold value) were becoming less frequent, the modest exceedance (approximately 15~30 μg/m^3 above the threshold values) was observed in more sites in recent years (Figure S7). The increase in the mean duration of O_3 extremes (Figure S8) also highlighted the nation-wide spread of O_3 pollution, among which BTH area showed the most significant growth, consistent with previous studies (Li et al. 2017a). The BTH is severely polluted with respect to $PM_{2.5}$, and mean exceedance days generally reached over 60 days (Figure 1c). The number of exceedances of $PM_{2.5}$ reached a daunting 150 days per year in 2013 to 2016 (Figure S9), which improved gradually since 2015 (He et al. 2020; Wang et al. 2020b; Xue et al. 2020), with both lower $PM_{2.5}$ levels (Figure S10) and lower severity observed (Figure S11). $PM_{2.5}$ exceedance days decreased at the rate of more than 10 days decade^{-1}, with the largest decreasing trend observed in BTH area (Figure 2c).

3.2 Changes in the joint exceedance of T_w, O_3 and $PM_{2.5}$

Figure 3 displays the trends of joint exceedance frequency of T_w, O_3 and $PM_{2.5}$ over the 2013–2020 period. Here, we identify an alarming trend of co-occurrence of T_w and O_3 extremes. High T_w and O_3 extremes tend to increase in the study period, especially in the BTH and YRD regions (at a rate up to 4.0 days decade^{-1}). Among exceedance days, mean duration and severity of T_w and O_3 co-occurrence, we observe similar spatiotemporal pattern, in which the rising trend of T_w and O_3 is larger individually than jointly (absolute changes, Figure S13 and S14), and most of the upward trend is observed in BTH and YRD regions driven by the co-occurrence in mid-summer (June and July, figures not shown).

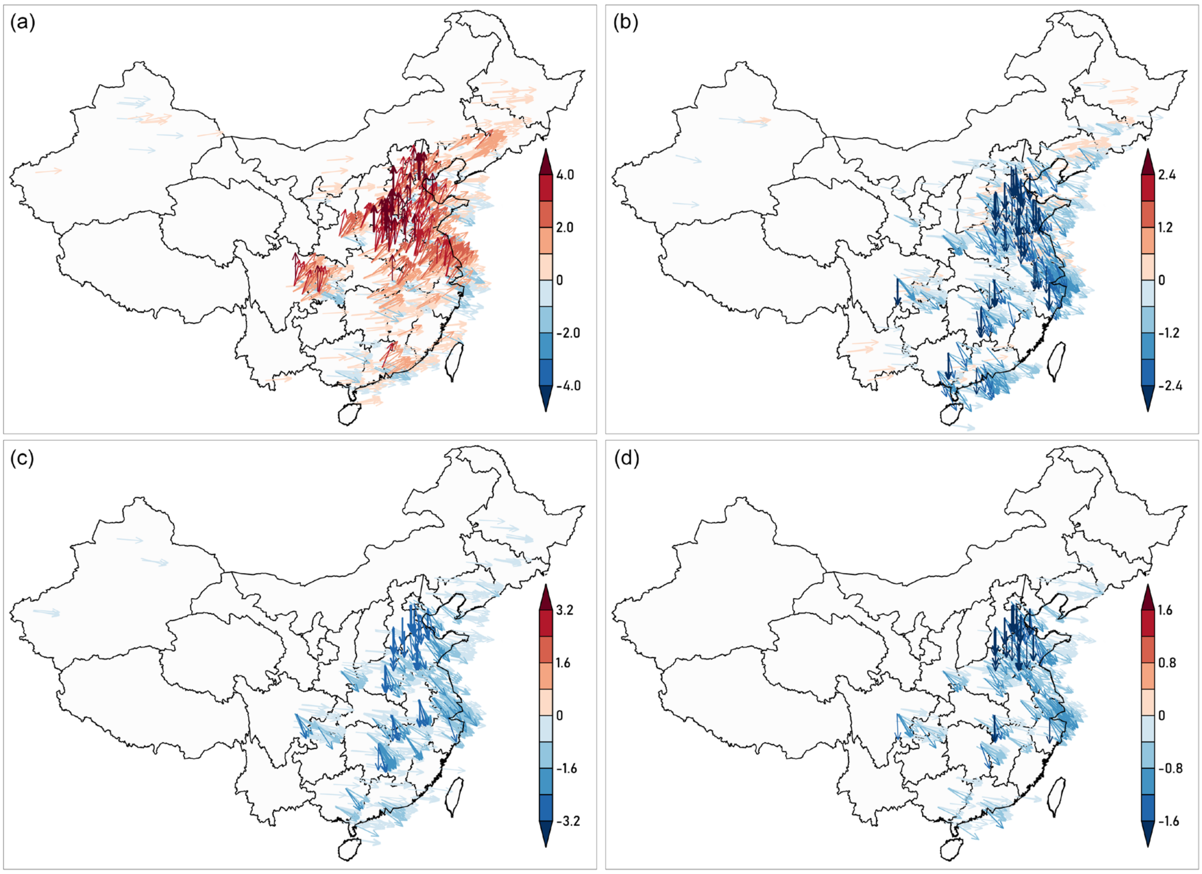

Fig. 3. Trend of co-occurrence of T_w, O_3 and $PM_{2.5}$ exceedance days over China. Co-occurrence of T_w and O_3 (a); co-occurrence of $PM_{2.5}$ and O_3 (b), T_w and $PM_{2.5}$ (c), T_w, $PM_{2.5}$ and O_3 (d). *Both the angle and color*

are showing the negative trends (i.e., downward sloping arrows in blue color) and positive trends (i.e., upward sloping arrows in red color)

The co-occurrence of O_3 extremes during heatwaves has long been recognized in developed countries (Filleul et al. 2006; Lee et al. 2006), and the underlying reason behind the combination of the two risk factors may partially be their common favorable weather patterns. For example, atmospheric blocking was reported to enhance the probability of co-occurrences of O_3 and heat extremes (Otero et al. 2021). Under a warming climate, amplified atmospheric blocking events are likely to lead to more frequent joint occurrences of heat and O_3 extremes (Nabizadeh et al. 2019). During heatwaves, the stagnant condition, controlled by anti-cyclone with a sinking airflow, may lead to less cloud cover (Pu et al. 2017) and weaker surface winds (Li et al. 2017b), both of which are favorable for O_3 formation (Pyrgou et al. 2018). Besides, previous review has indicated that high temperatures could play a catalytic role in promoting chemical reactions of O_3 formation and enhancing natural emissions of O_3 precursors; temperature is also associated with other synoptic patterns such as blocks and stagnation (Lu et al. 2019; Wang et al. 2017).

In addition, as NO_x and VOCs are not only precursors for O_3, but also important precursors for particular matter, anthropogenic emissions of NO_x, CO and volatile organic compounds (VOCs) could also play a role in the observed patterns (Logan 1985; Lu et al. 2018; Qu et al. 2014), which have indicated that both decreasing NO_x and increasing VOCs levels could enhance O_3 pollution. The finding was also replicated by recent studies in China (Gao et al. 2017; He et al. 2022) and US (Kim et al. 2016). Collectively, these studies revealed that when controlling the anthropogenic emission of NO_x, effective strategies of VOCs emission control should be also considered in high priority (He et al. 2022).

The co-occurrence of T_w, $PM_{2.5}$ and O_3 exceedance days had been decreasing at majority of sites, among which the greatest decreasing trend was observed in BTH (Figure 3d). The trend of duration of these co-extremes also showed a similar pattern (Figure S14). We observe that although $PM_{2.5}$ increased at a small number of sites (Figure 2c), the joint occurrence of $PM_{2.5}$ and O_3 is found to decrease at nearly all sites (Figure 3b). This is possibly associated with the fact that elevated $PM_{2.5}$ levels would reduce O_3 levels due to aerosols' influences on O_3 photochemistry and heterogeneous chemistry (Chen et al. 2020; Li et al. 2019).

In addition to the augmented cases (absolute changes) of co-occurrence of T_w and O_3, we ascertain in this study that the co-occurrence of T_w and O_3 have been increasing at higher percentage rates than the individual pace of each. As shown in Table 1, the exceedance days of T_w, and O_3 increased by 1.0 % decade^{-1}, 8.2 % decade^{-1}, respectively, while the joint exceedance of T_w and O_3 showed an augmented increase by 10.8 % decade^{-1}. Such an enhancement in the joint occurrences might be due to the abovementioned interaction between temperature and O_3 formation. Additionally, these numbers also indicate that although the co-occurrence of T_w and O_3 extremes was relatively rare in most cities, they have become more common in the recent years at a disproportionately larger rate.

Percentage change	Exceedance days			Mean duration		
	All	BTH	YRD	All	BTH	YRD
T_w	1.0%	0.9%	0.8%	9.1%	-59.4%	4.8%
O_3	8.2%	5.5%	6.6%	142.6%	92.1%	142.5%
$PM_{2.5}$	-3.8%	-12.0%	-10.9%	-28.2%	-82.9%	-97.1%
T_w & O_3	10.9%	7.0%	7.5%	112.2%	68.9%	139.0%
T_w & $PM_{2.5}$	-29.0%	-26.5%	-33.3%	-174.0%	-170.7%	305.4%
O_3 & $PM_{2.5}$	-28.6%	-21.1%	-33.9%	-86.0%	-183.5%	-148.8%
T_w, O_3 & $PM_{2.5}$	-24.8%	-22.2%	-28.5%	-127.0%	-142.3%	-190.3%

Table 1. Average trends in percentage per decade (calculated with respect to the mean levels of each metric over the study period).

3.3 Regional trend in BTH, YRD and PRD

Among the three regions, BTH showed the highest downward trend (-13.0 days decade^{-1}) in $PM_{2.5}$ exceedances, followed by YRD (-7.7 days decade^{-1}) and PRD (-4.6 days decade^{-1}) (Figure S15). Opposite trends were identified for O_3 exceedances, with BTH increasing at 11.4 days decade^{-1}, YRD increasing at 5.5 days decade^{-1} and PRD increasing at 1.7 days decade^{-1}. The exceedance trends of T_w were also positive, despite with a relatively smaller magnitude (0.9 days decade^{-1} for BTH, 3.8 days decade^{-1} for YRD and 4.3 days decade^{-1} for PRD) (Figure S15).

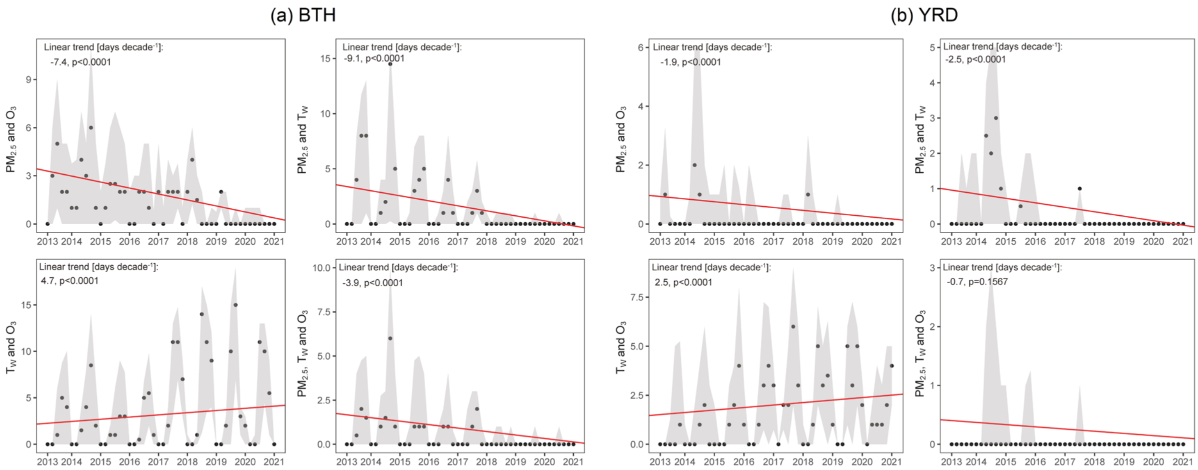

Fig. 4. Pooling trends of co-occurrence of T_w, O_3 and $PM_{2.5}$ exceedance days in BTH (a) and YRD (b) regions.

Since the co-occurrences of T_w, O_3 and $PM_{2.5}$ were relatively rare in the PRD region, next we only report results for the BTH and YRD. In the BTH, the co-occurrence of T_w and O_3 increased at 4.7 days decade^{-1} (or relatively at 7.0 %/decade) while all other combinations exhibited decreasing trends (Figure 4 and Figure 5a,). Similar patterns are found in the YRD (Figure 4 and Figure 5b). Similarly, increasing trends of T_w and O_3 severity and extreme duration were also identified in these two regions (Figure S16 and Figure S17). In BTH, we observe also that the exceedance days of T_w and O_3 co-extremes increased by 7.0%, higher than the percentage of each of them (0.9% and 5.5%, respectively, Table 1). Same amplification is also identified for the YRD.

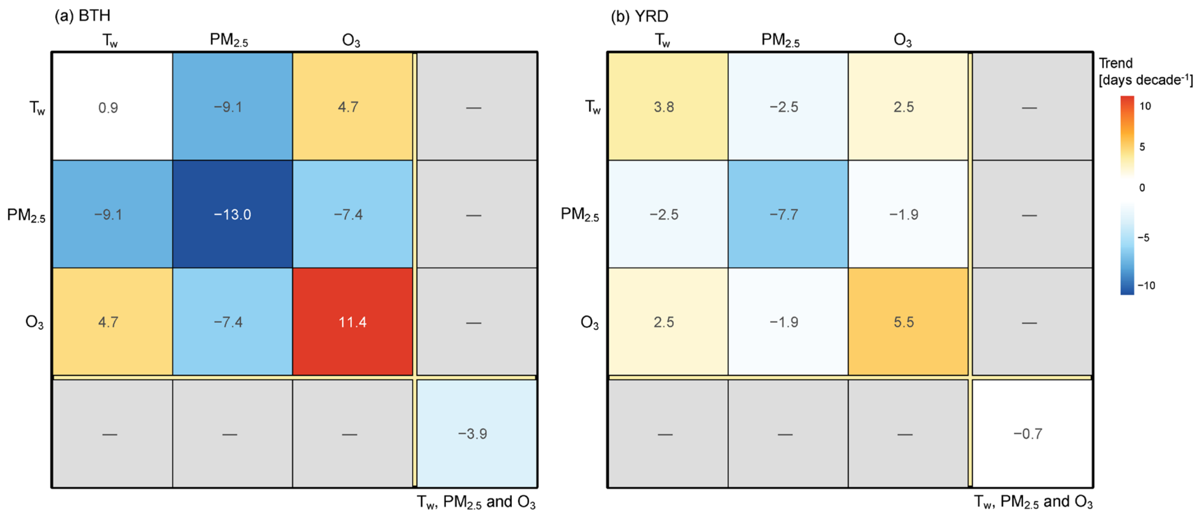

Fig. 5. Pooling trend of independent and joint occurrence of T_w, O_3 and $PM_{2.5}$ exceedance days in BTH (a), YRD (b).

3.4 Interpretation of the amplified trends

As there is no census on the definition of heatwaves around the globe. Previous studies that adopted various definitions of heatwaves have revealed differences of effect estimation under different definitions (Chen et al. 2015; Kent et al. 2014). Our study found that absolute changes in the rising trend of T_w and O_3 is larger individually than jointly while the percentage rates showed the opposite pattern. This counterintuitive result may be partially due to the small number of co-occurrence as we used the mean values of each metrics to derive the percentage change. In addition, the uncertainty of percentage change might also exist when using other definitions of heatwave. But our sensitivity analysis (Figure S21 and Figure S22) revealed that the direction and significance remain robust when using different threshold values. The amplified trend of T_w and O_3 we observed might be associated with multi-factors, such as urban growth, anthropogenic heat and $PM_{2.5}$ reduction. In addition, heatwaves trends were also suggested to be associated with the local hydroclimate (Liao et al. 2018). But we are unable to consider them in a multi-regression model as we do not have access to these data other than $PM_{2.5}$ that can be matched to each specific sites in this study. Another limitation of this study is that we used the fixed-effect model to obtain the average trend estimates in specific regions. The fixed-effect model made a assumption that the weight of trend in each site is simply determined by the corresponding variance residuals (lower indicating better model performance) of trend regression model. Other factors such as geographical and meteorological conditions (such as elevation and wind speed) of each site cannot be considered.

4 Conclusion

In the trend pooling analyses, we used a strategy to assess the overall trend of a particular region. The results are not sensitive to outliers in the time series of data. We first followed the trend analyses method proposed and used in previous studies (Chandler; Scott 2011; Cochrane; Orcutt 1949; Weatherhead et al. 1998), and then we combined the trend within regions by using a standard error-based weighting method. The results are consistent with previous studies. For example, contrasting trends of $PM_{2.5}$ and surface O_3 concentrations were observed among all of the three regions(Wang et al. 2020b). In addition, we also found that the severity of ozone pollution (difference between mean concentration and its threshold value) was also on the rise.

BTH, YRD and PRD are the three major city clusters in China and several studies have indicated that, in urban areas of these region, ozone formation is mainly VOC-limited or mixed-limited (Geng et al. 2009; Qu et al. 2014; Shao et al. 2009). For mixed-limited regions, it has been suggested that both decreasing NO_x levels and increasing VOCs levels could enhance ozone pollution (Lu et al. 2018). Furthermore, dealing with warming temperature and ozone pollution may have some co-benefits due to the relationship between temperature and ozone formation as discussed above as well as the fact that tropospheric ozone is a potent greenhouse gas. Therefore, cooperation in policies regarding warming climate and urban ozone pollution is warranted and further studies are needed to quantify the effect of emission control measures on both climate change and air pollution.

We conclude that China has achieved success in mitigating particulate matter pollution, as reduction in average concentration level, and in the frequency, duration and severity of exceedance events have been observed. However, the widespread ozone pollution and warming temperature as well as the less-recognized co-occurrence of these two conditions are on the rise across the country. These two damaging factors for public health and ecosystems (Chen et al. 2007; Rossati 2017) should be seen as an emerging alarming issue. Further investigation on both aspects is needed to develop control strategies that effectively mitigate the ongoing trend and avoid undesired consequences.

Acknowledgments

We acknowledge the European Centre for Medium-Range Weather Forecasts (ECWMF) for providing the ERA5 reanalysis datasets. This work was sponsored by Research Grants Council of the Hong Kong Special Administrative Region, China (project no. HKBU22201820).

Data Availability Statement

All the data presented can be accessed through contacting the corresponding authors.

REFERENCES

Basu, R., 2009: High ambient temperature and mortality: a review of epidemiologic studies from 2001 to 2008. *Environmental health*, **8,** 1-13.

Chandler, R., and M. Scott, 2011: *Statistical methods for trend detection and analysis in the environmental sciences.* John Wiley & Sons.

Chen, K., J. Bi, J. Chen, X. Chen, L. Huang, and L. Zhou, 2015: Influence of heat wave definitions to the added effect of heat waves on daily mortality in Nanjing, China. *Science of The Total Environment*, **506-507,** 18-25.

Chen, K., and Coauthors, 2018: Future ozone-related acute excess mortality under climate and population change scenarios in China: A modeling study. *PLOS Medicine*, **15,** e1002598.

Chen, S., H. Wang, K. Lu, L. Zeng, M. Hu, and Y. Zhang, 2020: The trend of surface ozone in Beijing from 2013 to 2019: Indications of the persisting strong atmospheric oxidation capacity. *Atmospheric Environment*, **242,** 117801.

Chen, T.-M., W. G. Kuschner, J. Gokhale, and S. Shofer, 2007: Outdoor Air Pollution: Ozone Health Effects. *The American Journal of the Medical Sciences*, **333,** 244-248.

Cochrane, D., and G. H. Orcutt, 1949: Application of least squares regression to relationships containing auto-correlated error terms. *Journal of the American statistical association*, **44,** 32-61.

Cohen, A. J., and Coauthors, 2017: Estimates and 25-year trends of the global burden of disease attributable to ambient air pollution: an analysis of data from the Global Burden of Diseases Study 2015. *The Lancet*, **389,** 1907-1918.

Dean, A., and D. Green, 2018: Climate change, air pollution and human health in Sydney, Australia: A review of the literature. *Environmental Research Letters*, **13,** 053003.

Dear, K., G. Ranmuthugala, T. Kjellström, C. Skinner, and I. Hanigan, 2005: Effects of temperature and ozone on daily mortality during the August 2003 heat wave in France. *Archives of environmental & occupational health*, **60,** 205-212.

Ding, T., W. Qian, and Z. Yan, 2010: Changes in hot days and heat waves in China during 1961–2007. *International Journal of Climatology*, **30,** 1452-1462.

Ebi, K. L., and G. McGregor, 2008: Climate change, tropospheric ozone and particulate matter, and health impacts. *Environmental health perspectives*, **116,** 1449-1455.

Field, C. B., V. Barros, T. F. Stocker, and Q. Dahe, 2012: *Managing the risks of extreme events and* *disasters to advance climate change adaptation: special report of the intergovernmental panel on climate change.* Cambridge University Press.

Filleul, L., and Coauthors, 2006: The relation between temperature, ozone, and mortality in nine French cities during the heat wave of 2003. *Environmental health perspectives*, **114,** 1344-1347.

Gao, M., and Coauthors, 2020a: China's emission control strategies have suppressed unfavorable influences of climate on wintertime PM 2.5 concentrations in Beijing since 2002. *Atmospheric Chemistry and Physics*, **20,** 1497-1505.

Gao, M., and Coauthors, 2020b: Ozone pollution over China and India: seasonality and sources. *Atmospheric Chemistry and Physics*, **20,** 4399-4414.

Gao, W., X. Tie, J. Xu, R. Huang, X. Mao, G. Zhou, and L. Chang, 2017: Long-term trend of O3 in a mega City (Shanghai), China: Characteristics, causes, and interactions with precursors. *Science of The Total Environment*, **603-604,** 425-433.

Geng, F., and Coauthors, 2009: Aircraft measurements of O3, NOx, CO, VOCs, and SO2 in the Yangtze River Delta region. *Atmospheric Environment*, **43,** 584-593.

Gerosa, G., A. Finco, S. Mereu, M. Vitale, F. Manes, and A. B. Denti, 2009: Comparison of seasonal variations of ozone exposure and fluxes in a Mediterranean Holm oak forest between the exceptionally dry 2003 and the following year. *Environmental Pollution*, **157,** 1737-1744.

He, Q., Y. Gu, and M. Zhang, 2020: Spatiotemporal trends of PM2.5 concentrations in central China from 2003 to 2018 based on MAIAC-derived high-resolution data. *Environment International*, **137,** 105536.

He, Z., P. Liu, X. Zhao, X. He, J. Liu, and Y. Mu, 2022: Responses of surface O3 and PM2.5 trends to changes of anthropogenic emissions in summer over Beijing during 2014–2019: A study based on multiple linear regression and WRF-Chem. *Science of The Total Environment*, **807,** 150792.

Hersbach, H., and Coauthors, 2020: The ERA5 global reanalysis. *Quarterly Journal of the Royal Meteorological Society*, **146,** 1999-2049.

Jia, M., and Coauthors, 2017: Inverse relations of PM2. 5 and O3 in air compound pollution between cold and hot seasons over an urban area of east China. *Atmosphere*, **8,** 59.

Kan, H., R. Chen, and S. Tong, 2012: Ambient air pollution, climate change, and population health in China. *Environment international*, **42,** 10-19.

Karl, T., A. Guenther, C. Spirig, A. Hansel, and R. Fall, 2003: Seasonal variation of biogenic VOC emissions above a mixed hardwood forest in northern Michigan. *Geophysical Research Letters*, **30**.

Kent, S. T., L. A. McClure, B. F. Zaitchik, T. T. Smith, and J. M. Gohlke, 2014: Heat Waves and Health Outcomes in Alabama (USA): The Importance of Heat Wave Definition. *Environmental Health Perspectives*, **122,** 151-158.

Kim, S.-W., and Coauthors, 2016: Modeling the weekly cycle of NOx and CO emissions and their impacts on O3 in the Los Angeles-South Coast Air Basin during the CalNex 2010 field campaign. *Journal of Geophysical Research: Atmospheres*, **121,** 1340-1360.

Kinney, P. L., 2008: Climate change, air quality, and human health. *American journal of preventive medicine*, **35,** 459-467.

Knutson, T. R., and J. J. Ploshay, 2016: Detection of anthropogenic influence on a summertime heat stress index. *Climatic Change*, **138,** 25-39.

Kovats, R. S., and S. Hajat, 2008: Heat stress and public health: a critical review. *Annu. Rev. Public Health*, **29,** 41-55.

Lee, J. D., and Coauthors, 2006: Ozone photochemistry and elevated isoprene during the UK heatwave of august 2003. *Atmospheric Environment*, **40,** 7598-7613.

Li, G., L. Jiang, Y. Zhang, Y. Cai, X. Pan, and M. Zhou, 2014: The impact of ambient particle pollution during extreme-temperature days in Guangzhou City, China. *Asia Pacific Journal of Public Health*, **26,** 614-621.

Li, G., and Coauthors, 2017a: Widespread and persistent ozone pollution in eastern China during the non-winter season of 2015: observations and source attributions. *Atmos. Chem. Phys.*, **17,** 2759-2774.

Li, K., D. J. Jacob, H. Liao, L. Shen, Q. Zhang, and K. H. Bates, 2019: Anthropogenic drivers of 2013–2017 trends in summer surface ozone in China. *Proceedings of the National Academy of Sciences*, **116,** 422-427.

Li, K., and Coauthors, 2017b: Meteorological and chemical impacts on ozone formation: A case study in Hangzhou, China. *Atmospheric Research*, **196,** 40-52.

Liang, F., M. Gao, Q. Xiao, G. R. Carmichael, X. Pan, and Y. Liu, 2017: Evaluation of a data fusion approach to estimate daily PM2. 5 levels in North China. *Environmental research*, **158,** 54-60.

Liao, W., and Coauthors, 2018: Stronger Contributions of Urbanization to Heat Wave Trends in Wet Climates. *Geophysical Research Letters*, **45,** 11,310-311,317.

Lin, C. Q., G. Liu, A. K. H. Lau, Y. Li, C. C. Li, J. C. H. Fung, and X. Q. Lao, 2018: High-resolution satellite remote sensing of provincial PM2.5 trends in China from 2001 to 2015. *Atmospheric Environment*, **180,** 110-116.

Lin, M., and Coauthors, 2020: Vegetation feedbacks during drought exacerbate ozone air pollution extremes in Europe. *Nature Climate Change*, **10,** 444-451.

Lipsey, M. W., and D. B. Wilson, 2001: *Practical meta-analysis.* SAGE publications, Inc.

Liu, H., J. Liao, D. Yang, X. Du, P. Hu, Y. Yang, and B. Li, 2014: The response of human thermal perception and skin temperature to step-change transient thermal environments. *Building and environment*, **73,** 232-238.

Liu, H., and Coauthors, 2018: Ground-level ozone pollution and its health impacts in China. *Atmospheric Environment*, **173,** 223-230.

Liu, Y., and T. Wang, 2020: Worsening urban ozone pollution in China from 2013 to 2017 – Part 1: The complex and varying roles of meteorology. *Atmos. Chem. Phys.*, **20,** 6305-6321.

Logan, J. A., 1985: Tropospheric ozone: Seasonal behavior, trends, and anthropogenic influence. *Journal of Geophysical Research: Atmospheres*, **90,** 10463-10482.

Lu, X., L. Zhang, and L. Shen, 2019: Meteorology and climate influences on tropospheric ozone: a review of natural sources, chemistry, and transport patterns. *Current Pollution Reports*, **5,** 238-260.

Lu, X., and Coauthors, 2020: Rapid Increases in Warm-Season Surface Ozone and Resulting Health Impact in China Since 2013. *Environmental Science & Technology Letters*, **7,** 240-247.

Lu, X., and Coauthors, 2018: Severe surface ozone pollution in China: a global perspective. *Environmental Science & Technology Letters*, **5,** 487-494.

Ma, X., H. Jia, T. Sha, J. An, and R. Tian, 2019: Spatial and seasonal characteristics of particulate matter and gaseous pollution in China: Implications for control policy. *Environmental Pollution*, **248,** 421-428.

Mora, C., and Coauthors, 2017: Global risk of deadly heat. *Nature climate change*, **7,** 501-506.

Nabizadeh, E., P. Hassanzadeh, D. Yang, and E. A. Barnes, 2019: Size of the atmospheric blocking events: Scaling law and response to climate change. *Geophysical Research Letters*, **46,** 13488-13499.

Otero, N., O. Jurado, T. Butler, and H. W. Rust, 2021: The impact of atmospheric blocking on the compounding effect of ozone pollution and temperature: A copula-based approach. *Atmospheric*

Chemistry and Physics Discussions, 1-17.

Pachauri, R. K., and Coauthors, 2014: *Climate change 2014: synthesis report. Contribution of Working Groups I, II and III to the fifth assessment report of the Intergovernmental Panel on Climate Change.* Ipcc.

Pu, X., T. J. Wang, X. Huang, D. Melas, P. Zanis, D. K. Papanastasiou, and A. Poupkou, 2017: Enhanced surface ozone during the heat wave of 2013 in Yangtze River Delta region, China. *Science of The Total Environment*, **603-604,** 807-816.

Pyrgou, A., P. Hadjinicolaou, and M. Santamouris, 2018: Enhanced near-surface ozone under heatwave conditions in a Mediterranean island. *Scientific Reports*, **8,** 9191.

Qu, Y., J. An, J. Li, Y. Chen, Y. Li, X. Liu, and M. Hu, 2014: Effects of NOxand VOCs from five emission sources on summer surface O3 over the Beijing-Tianjin-Hebei region. *Advances in Atmospheric Sciences*, **31,** 787-800.

Ren, C., G. M. Williams, L. Morawska, K. Mengersen, and S. Tong, 2008: Ozone modifies associations between temperature and cardiovascular mortality: analysis of the NMMAPS data. *Occupational and environmental medicine*, **65,** 255-260.

Rossati, A., 2017: Global warming and its health impact. *The international journal of occupational and environmental medicine*, **8,** 7.

Russo, S., J. Sillmann, and A. Sterl, 2017: Humid heat waves at different warming levels. *Scientific reports*, **7,** 1-7.

Sánchez-Meca, J., and F. Marín-Martínez, 2010: Meta Analysis. *International Encyclopedia of Education (Third Edition)*, P. Peterson, E. Baker, and B. McGaw, Eds., Elsevier, 274-282.

Sanderson, M. G., D. L. Hemming, and R. A. Betts, 2011: Regional temperature and precipitation changes under high-end (≥4°C) global warming. *Philosophical Transactions of the Royal Society A: Mathematical, Physical and Engineering Sciences*, **369,** 85-98.

Shao, M., Y. Zhang, L. Zeng, X. Tang, J. Zhang, L. Zhong, and B. Wang, 2009: Ground-level ozone in the Pearl River Delta and the roles of VOC and NOx in its production. *Journal of Environmental Management*, **90,** 512-518.

Sherwood, S. C., 2018: How important is humidity in heat stress? *Journal of Geophysical Research: Atmospheres*, **123,** 11,808-811,810.

Stafoggia, M., J. Schwartz, F. Forastiere, and C. Perucci, 2008: Does temperature modify the association between air pollution and mortality? A multicity case-crossover analysis in Italy. *American journal of epidemiology*, **167,** 1476-1485.

Stull, R., 2011: Wet-bulb temperature from relative humidity and air temperature. *Journal of applied meteorology and climatology*, **50,** 2267-2269.

Wang, Q., and Coauthors, 2020a: Independent and Combined Effects of Heatwaves and PM2.5 on Preterm Birth in Guangzhou, China: A Survival Analysis. *Environmental Health Perspectives*, **128,** 017006.

Wang, T., L. Xue, P. Brimblecombe, Y. F. Lam, L. Li, and L. Zhang, 2017: Ozone pollution in China: A review of concentrations, meteorological influences, chemical precursors, and effects. *Science of The Total Environment*, **575,** 1582-1596.

Wang, Y., and Coauthors, 2020b: Contrasting trends of PM2.5 and surface-ozone concentrations in China from 2013 to 2017. *National Science Review*, **7,** 1331-1339.

Wang, Z., and Coauthors, 2021: Incorrect Asian aerosols affecting the attribution and projection of regional climate change in CMIP6 models. *npj Climate and Atmospheric Science*, **4,** 1-8.

Watts, N., and Coauthors, 2015: Health and climate change: policy responses to protect public health. *The Lancet*, **386,** 1861-1914.

Weatherhead, E. C., and Coauthors, 1998: Factors affecting the detection of trends: Statistical considerations and applications to environmental data. *Journal of Geophysical Research: Atmospheres*, **103,** 17149-17161.

Wei, K., and W. Chen, 2011: An abrupt increase in the summer high temperature extreme days across China in the mid-1990s. *Advances in Atmospheric Sciences*, **28,** 1023-1029.

WHO, 2020: Air pollution, World Health Organization.

Willers, S. M., and Coauthors, 2016: High resolution exposure modelling of heat and air pollution and the impact on mortality. *Environment international*, **89,** 102-109.

Willett, K. M., and S. Sherwood, 2012: Exceedance of heat index thresholds for 15 regions under a warming climate using the wet-bulb globe temperature. *International Journal of Climatology*, **32,** 161-177.

Xu, Y., J.-F. Lamarque, and B. M. Sanderson, 2018: The importance of aerosol scenarios in projections of future heat extremes. *Climatic Change*, **146,** 393-406.

Xu, Y., and Coauthors, 2020: Substantial Increase in the Joint Occurrence and Human Exposure of

Heatwave and High-PM Hazards Over South Asia in the Mid-21st Century. *AGU Advances*, **1,** e2019AV000103.

Xue, W., J. Zhang, C. Zhong, D. Ji, and W. Huang, 2020: Satellite-derived spatiotemporal PM2.5 concentrations and variations from 2006 to 2017 in China. *Science of The Total Environment*, **712,** 134577.

Zanobetti, A., and A. Peters, 2015: Disentangling interactions between atmospheric pollution and weather. BMJ Publishing Group Ltd.

Zhang, Q., and Coauthors, 2019: Drivers of improved PM2. 5 air quality in China from 2013 to 2017. *Proceedings of the National Academy of Sciences*, **116,** 24463-24469.

Zhang, Y., P. Yang, Y. Gao, R. L. Leung, and M. L. Bell, 2020: Health and economic impacts of air pollution induced by weather extremes over the continental US. *Environment International*, **143,** 105921.

Zhao, B., Y. Su, S. He, M. Zhong, and G. Cui, 2016: Evolution and comparative assessment of ambient air quality standards in China. *Journal of Integrative Environmental Sciences*, **13,** 85-102.

Zheng, M., L. G. Salmon, J. J. Schauer, L. Zeng, C. Kiang, Y. Zhang, and G. R. Cass, 2005: Seasonal trends in PM2. 5 source contributions in Beijing, China. *Atmospheric Environment*, **39,** 3967-3976.

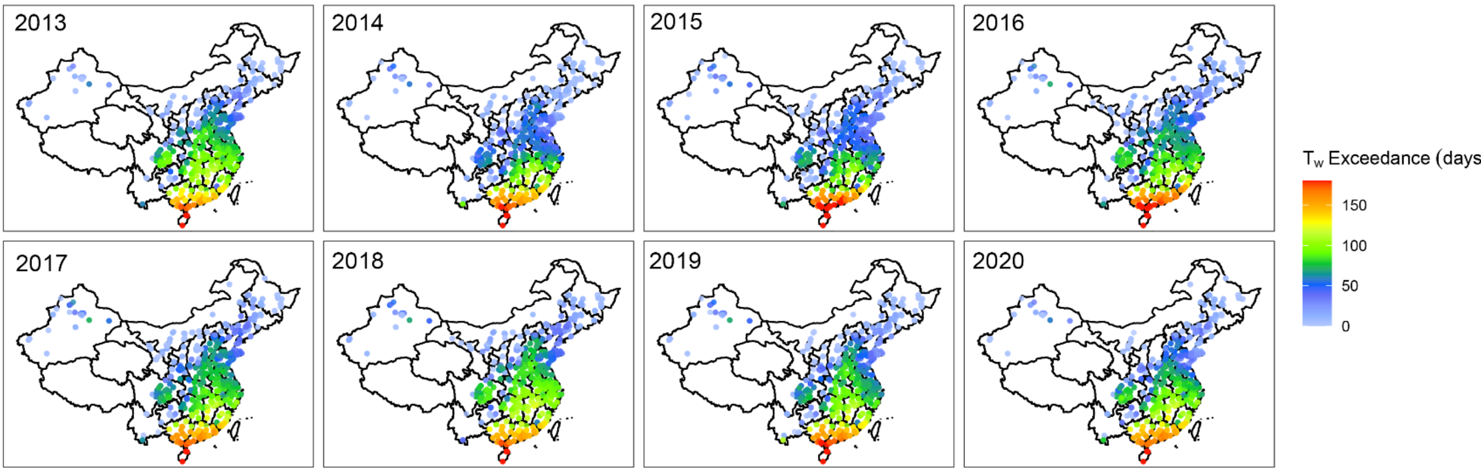

Figure S1. Number of T_w exceedance days across China over 2013–2020.

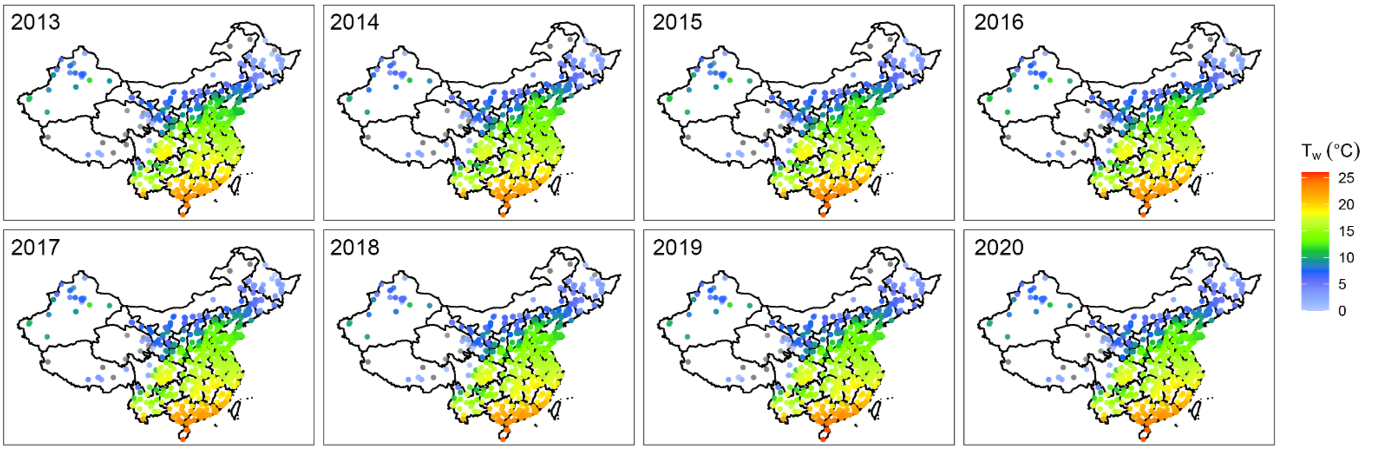

Figure S2. Average T_w across China over 2013–2020 (°C).

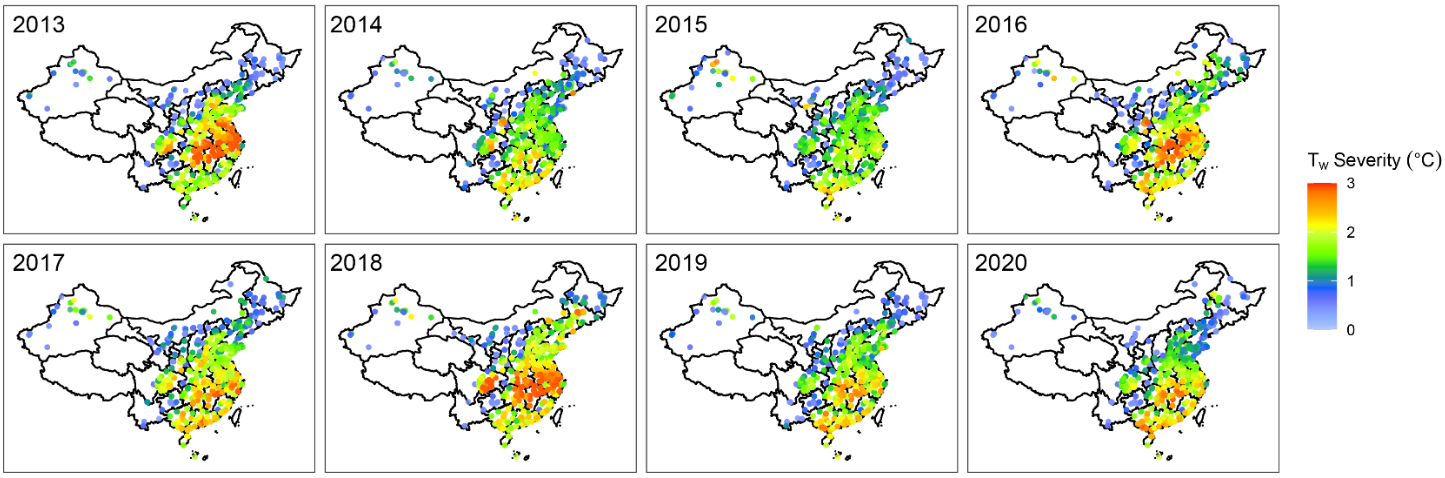

Figure S3. T_w severity across China over 2013–2020.

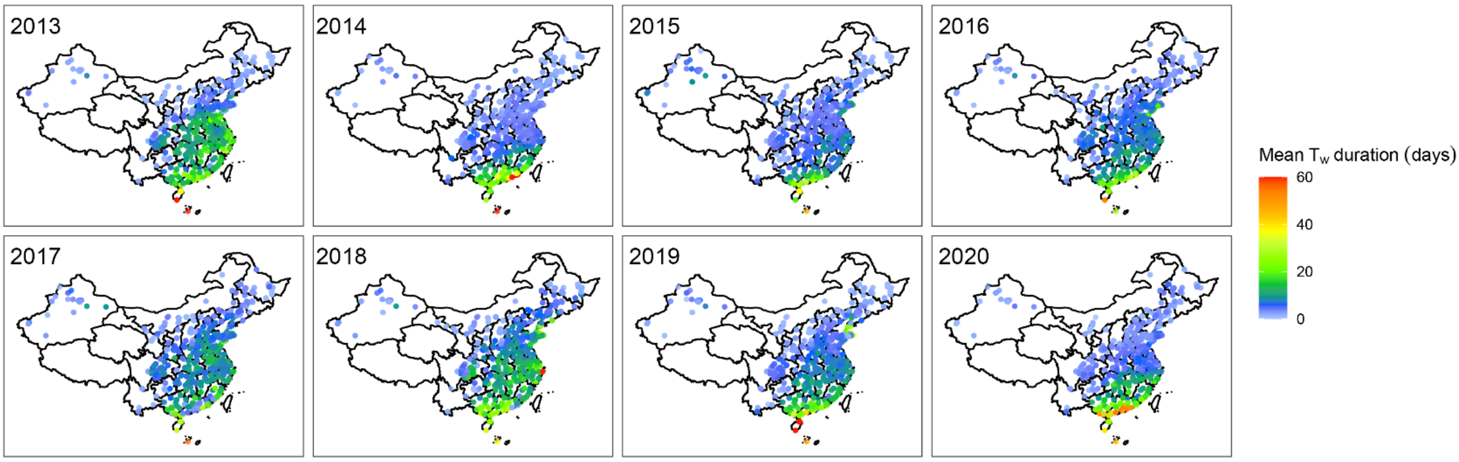

Figure S4. Mean T_w extremes duration across China over 2013–2020

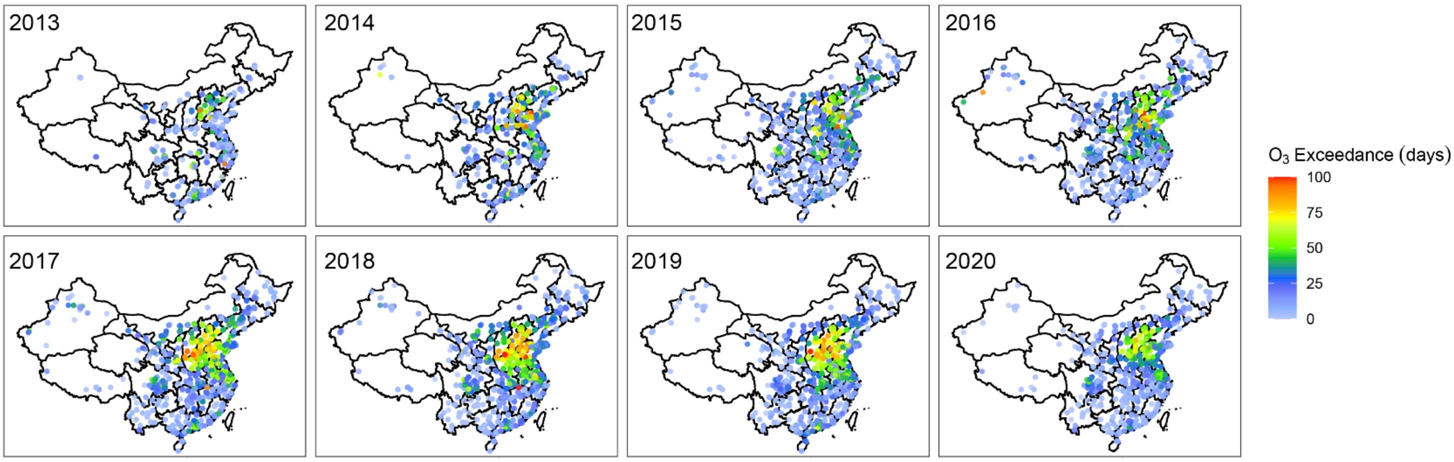

Figure S5. Number of O_3 exceedance days across China over 2013–2020.

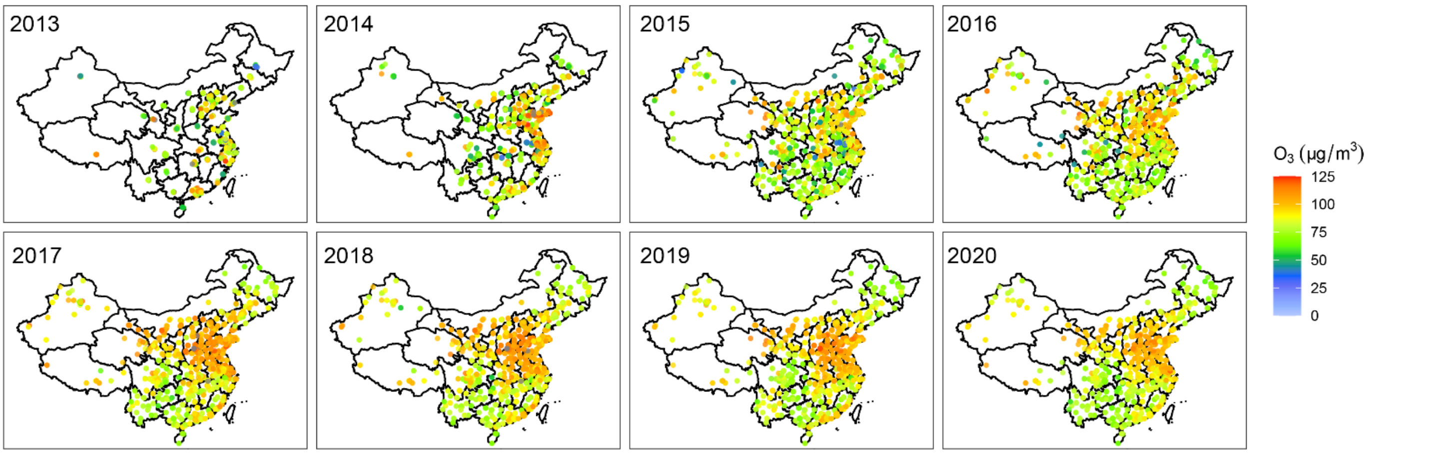

Figure S6. Average O_3 levels across China over 2013–2020.

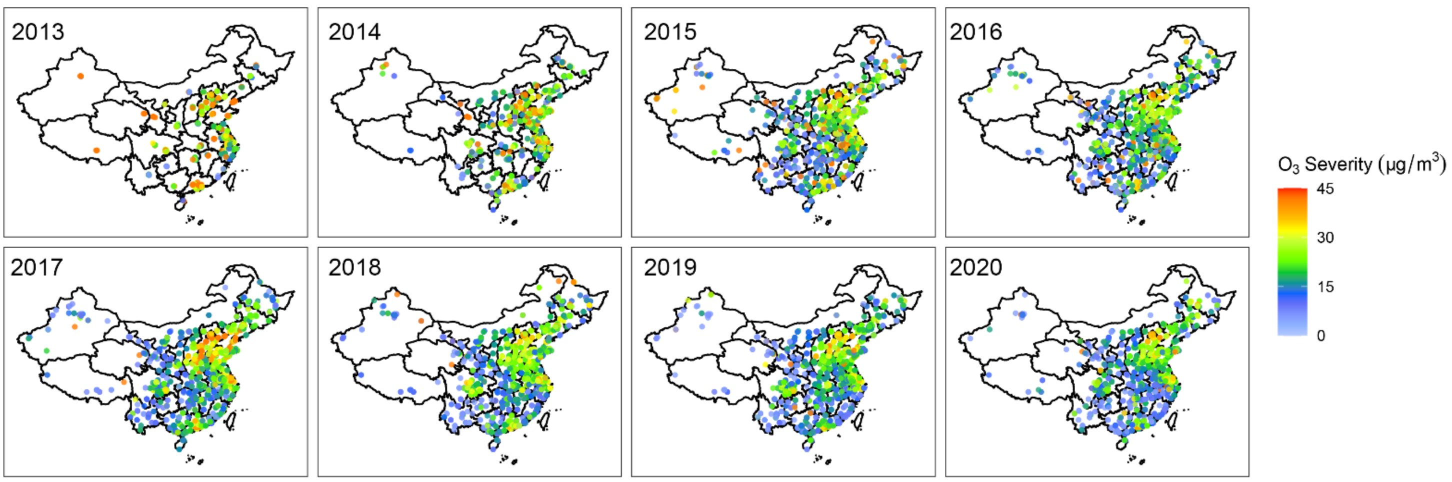

Figure S7. O_3 severity across China over 2013–2020.

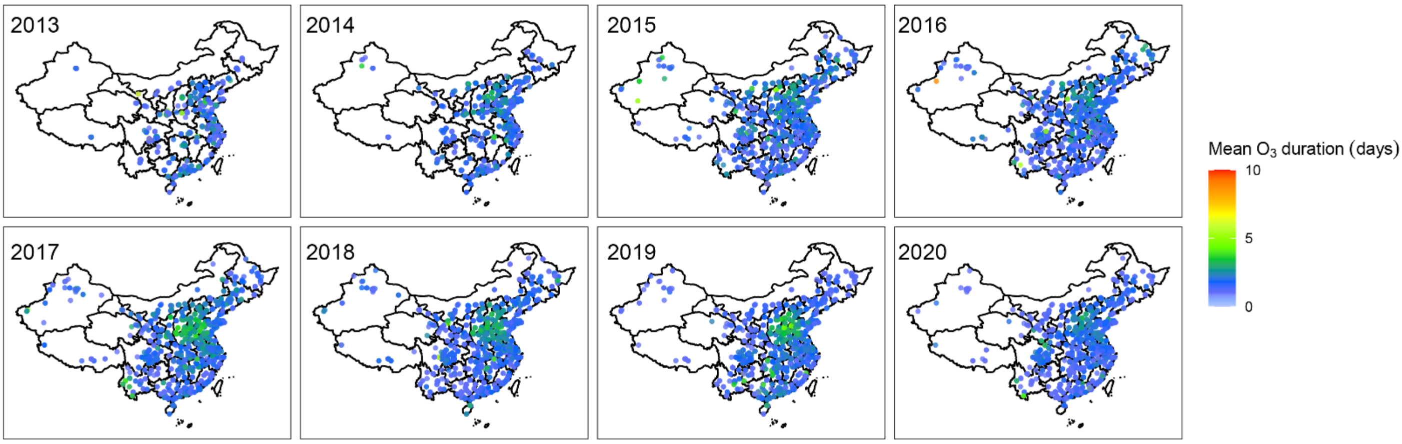

Figure S8. Mean O_3 extremes duration across China over 2013–2020.

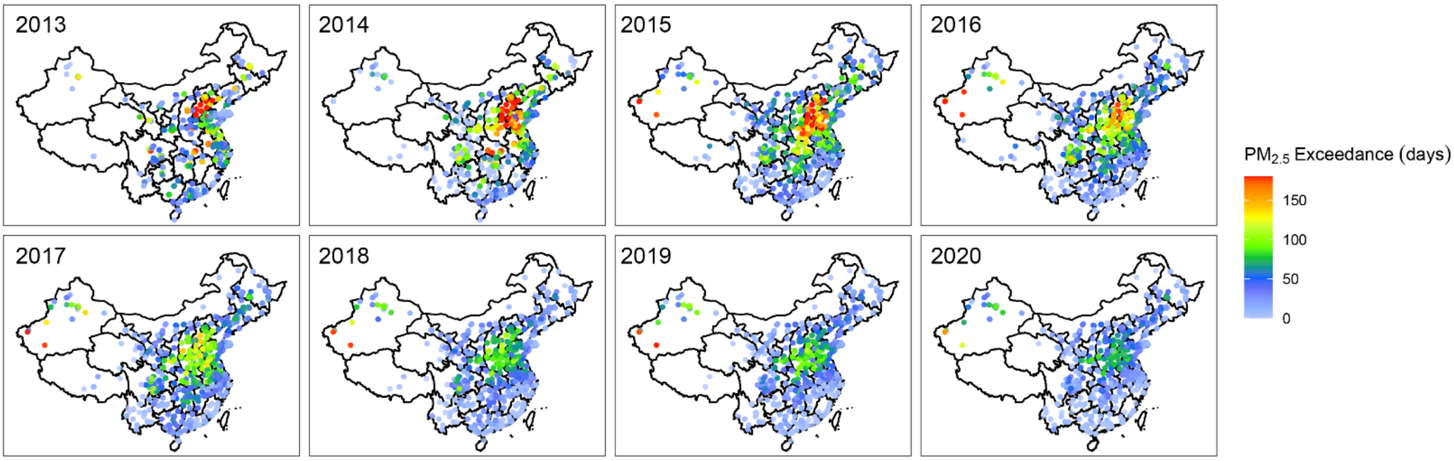

Figure S9. Number of $PM_{2.5}$ exceedance days across China over 2013–2020.

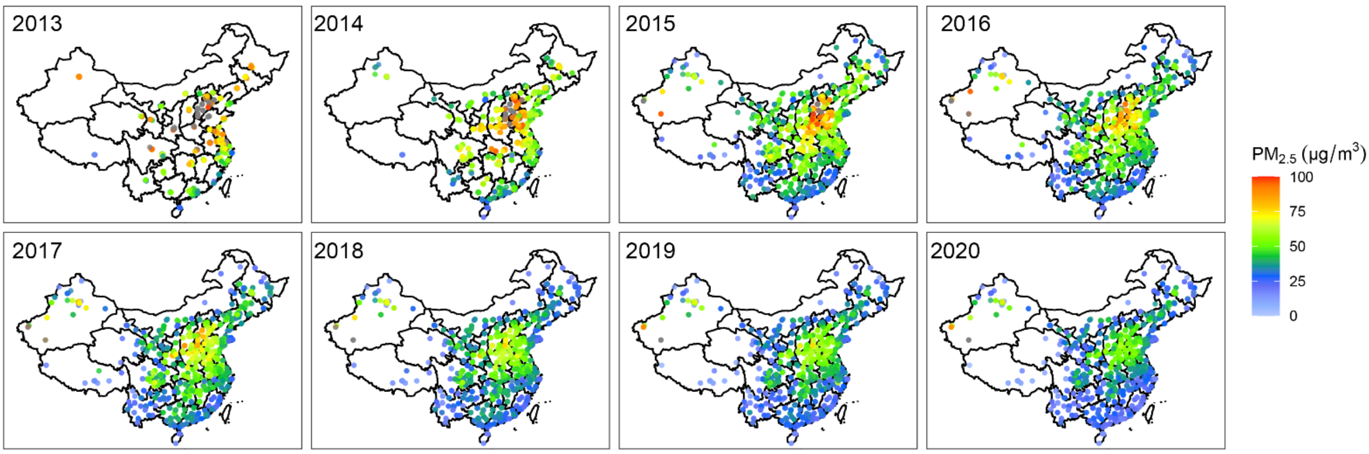

Figure S10. Average $PM_{2.5}$ levels across China over 2013–2020.

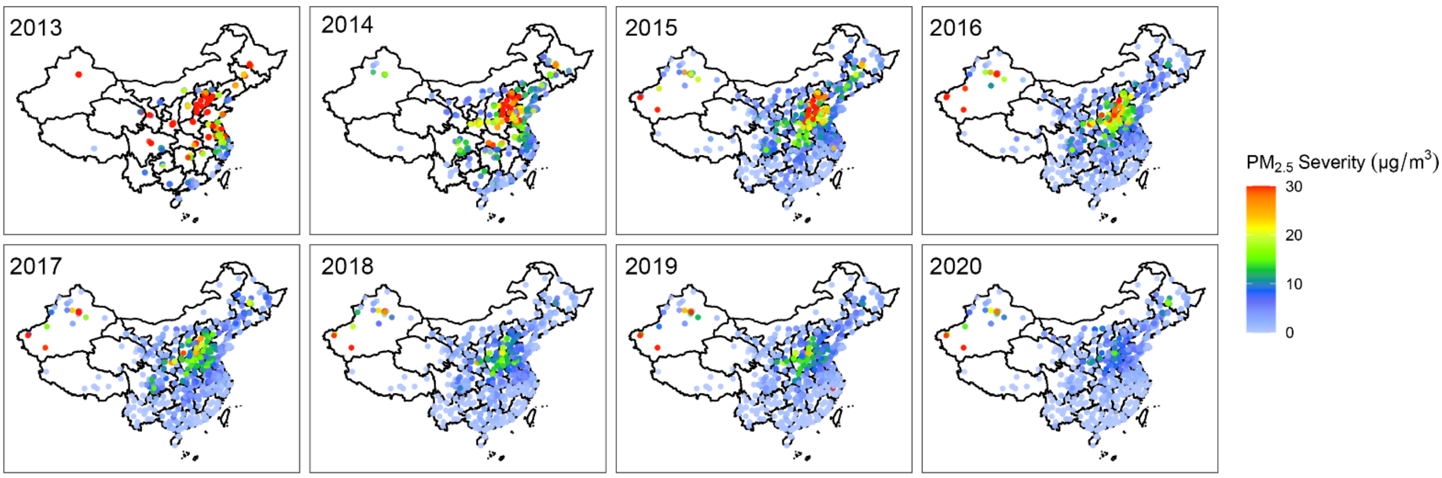

Figure S11. $PM_{2.5}$ severity across China over 2013–2020.

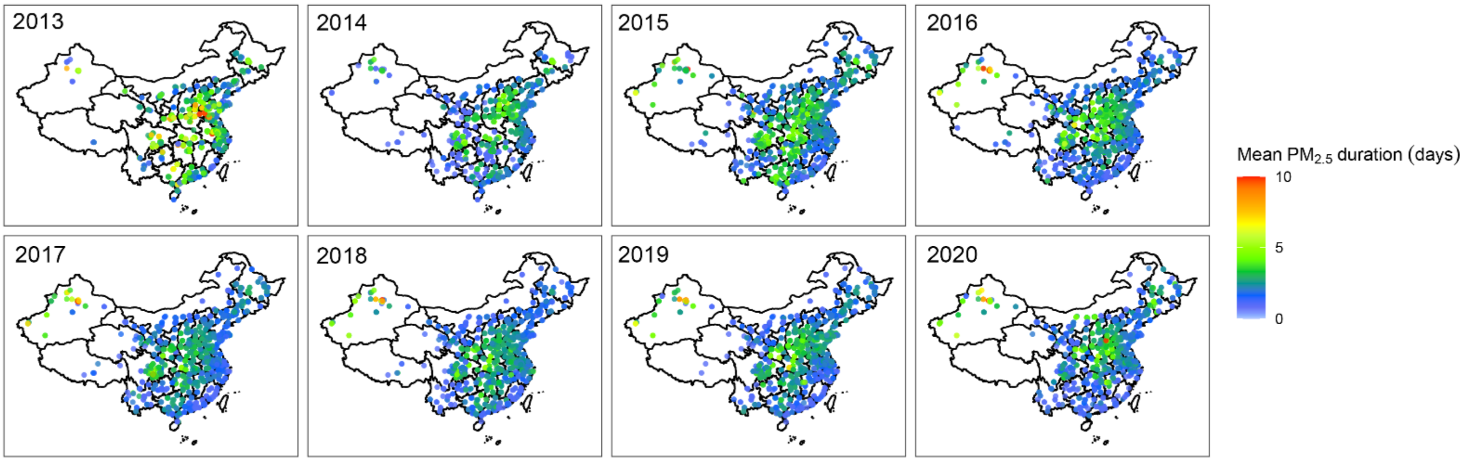

Figure S12. Mean $PM_{2.5}$ extremes duration across China over 2013–2020.

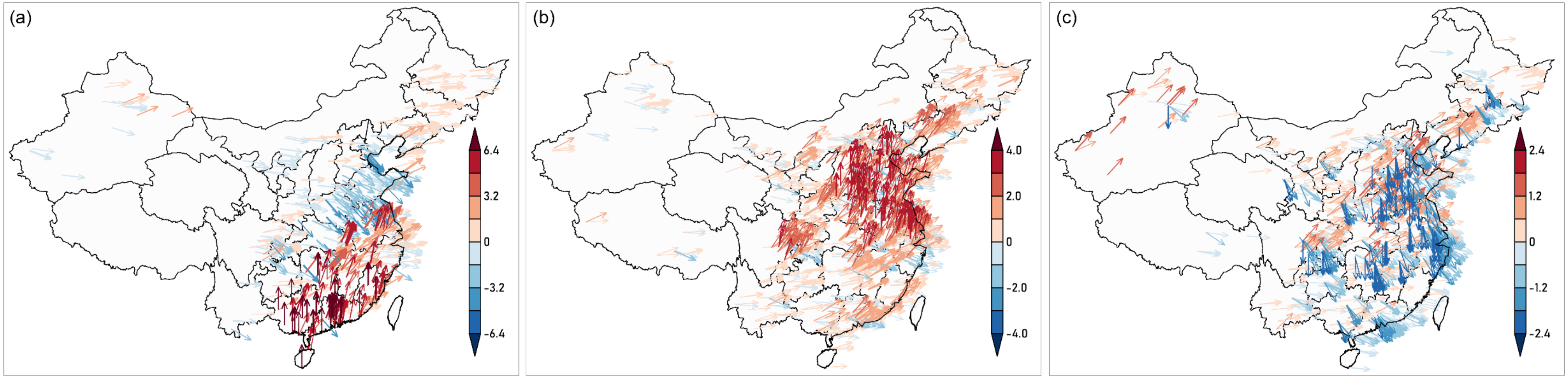

Figure S13. Trend of mean duration of T_w (a), O_3 (b) and $PM_{2.5}$ (c) extremes (days decade^{-1}).

Footnote: Both the angle and color are showing the negative trends (i.e., downward sloping arrows in blue color) and positive trends (i.e., upward sloping arrows in red color)

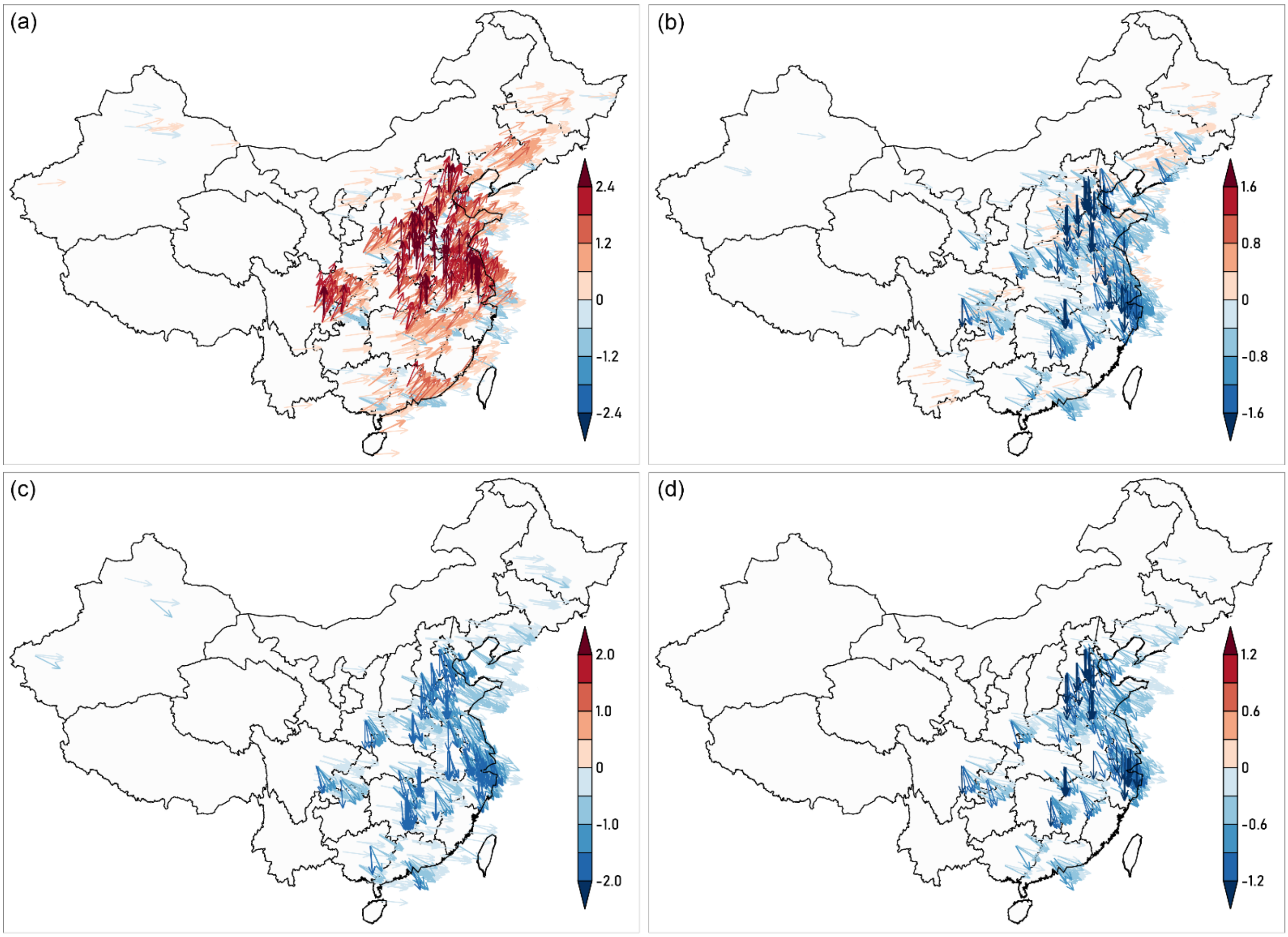

Figure S14. Trend of mean duration of co-occurrence of T_w, O_3 and $PM_{2.5}$ extremes. Co-occurrence of T_w and O_3 (a); co-occurrence of $PM_{2.5}$ and O_3 (b), T_w and $PM_{2.5}$ (c), T_w , $PM_{2.5}$ and O_3 (d).

Footnote: Both the angle and color are showing the negative trends (i.e., downward sloping arrows in blue color) and positive trends (i.e., upward sloping arrows in red color)

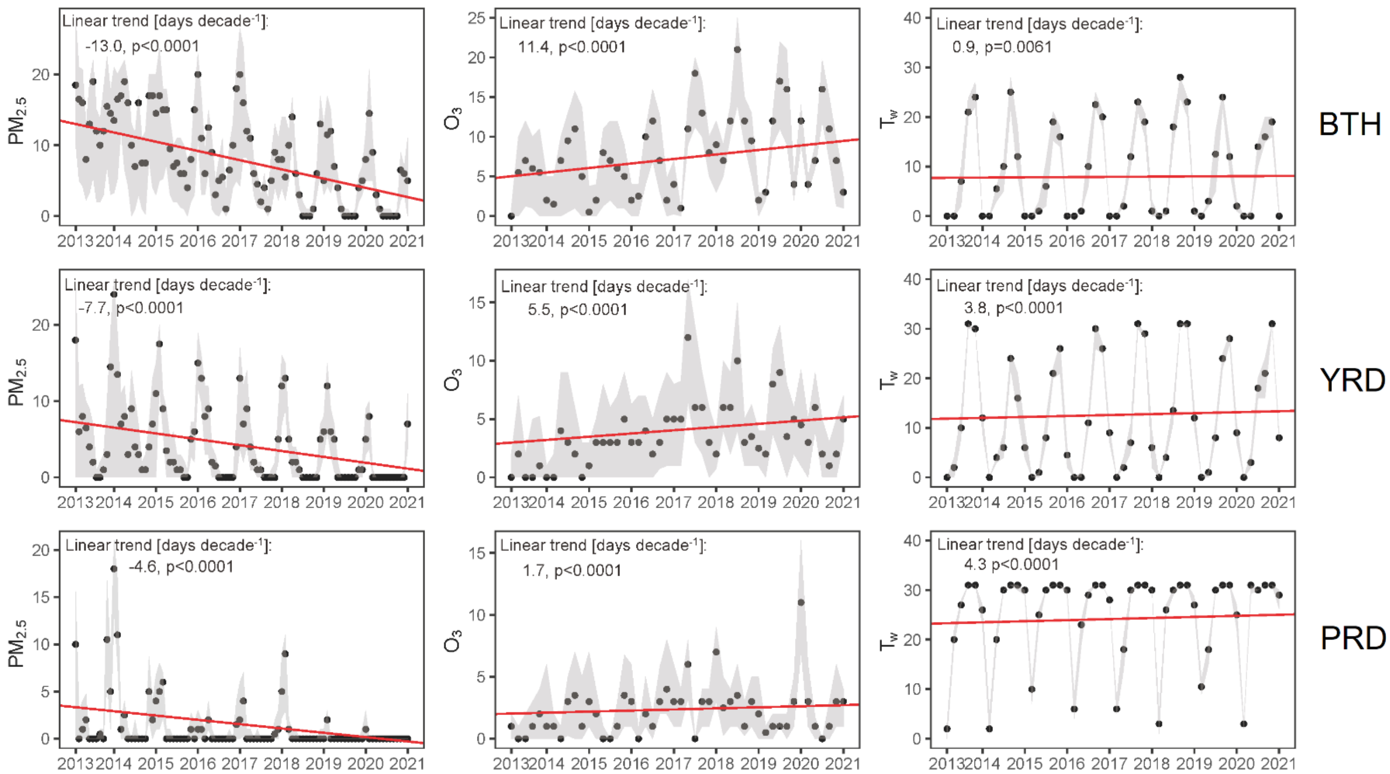

Figure S15. Pooling trend of T_w, O_3 and $PM_{2.5}$ exceedance days in BTH, YRD and PRD regions.

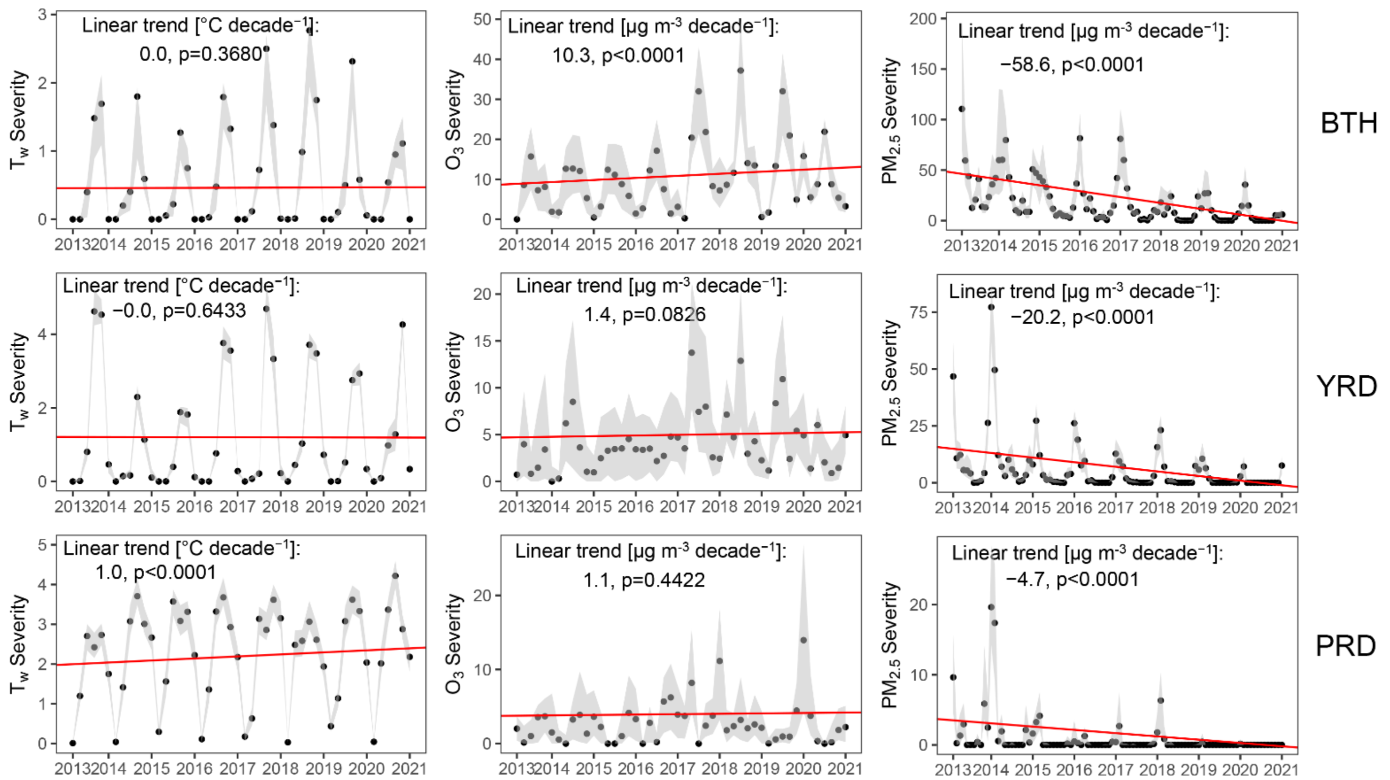

Figure S16. Pooling trend of T_w, O_3 and $PM_{2.5}$ severity in BTH, YRD and PRD regions.

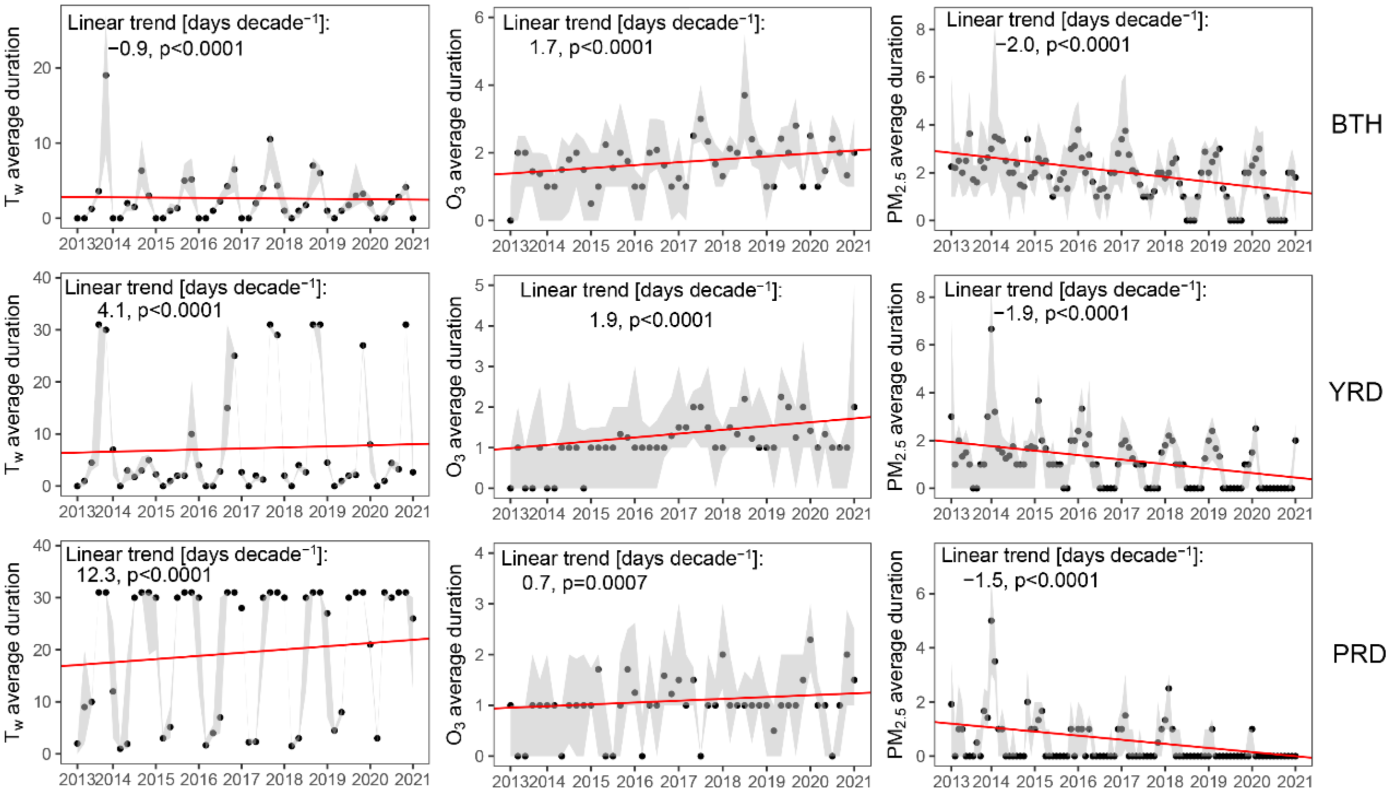

Figure S17. Pooling trend of T_w, O_3 and $PM_{2.5}$ average durations in BTH, YRD and PRD regions.

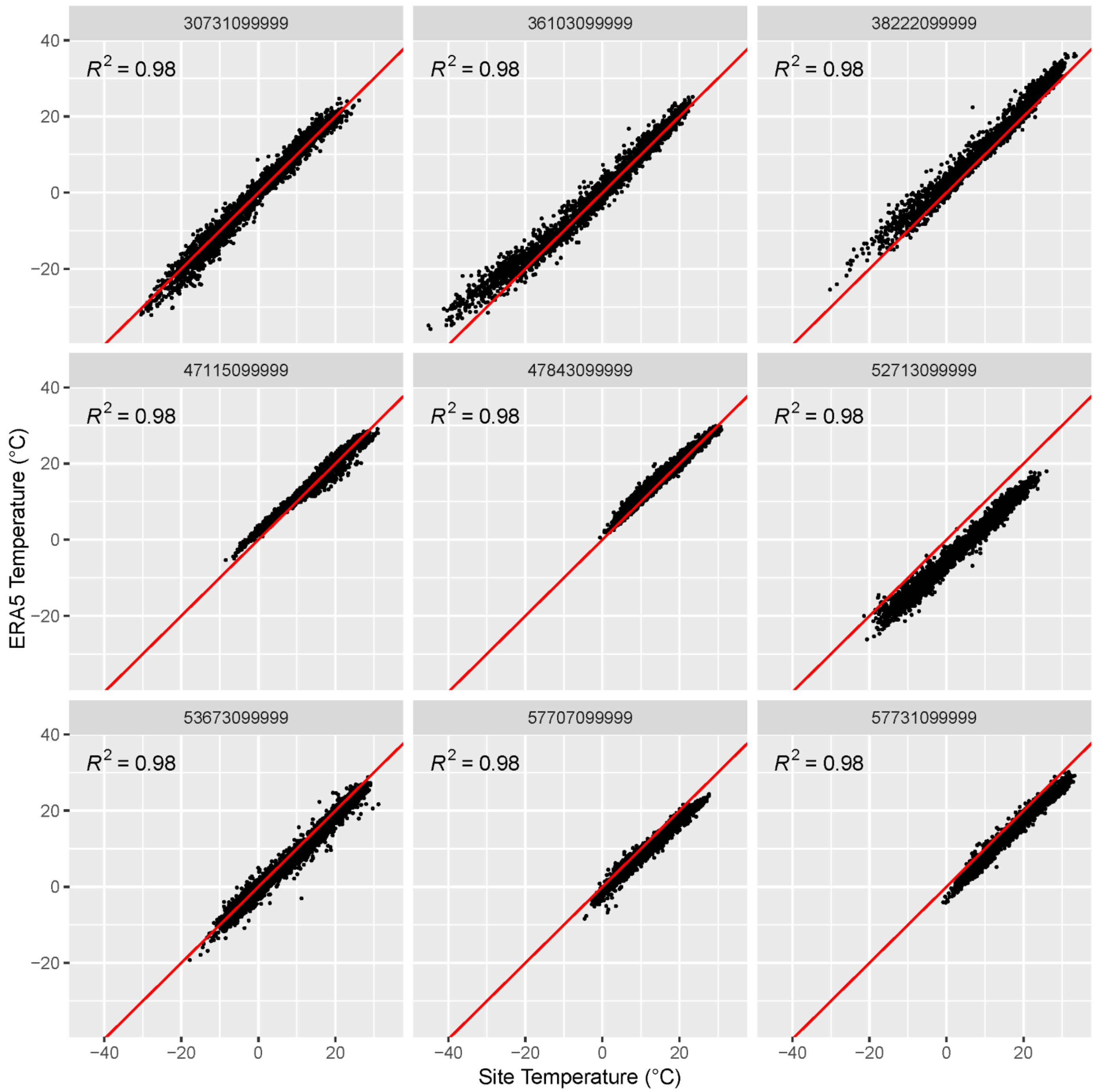

Figure S18. The scatterplot of site and ERA5 temperature (sites with median correlation coefficients)

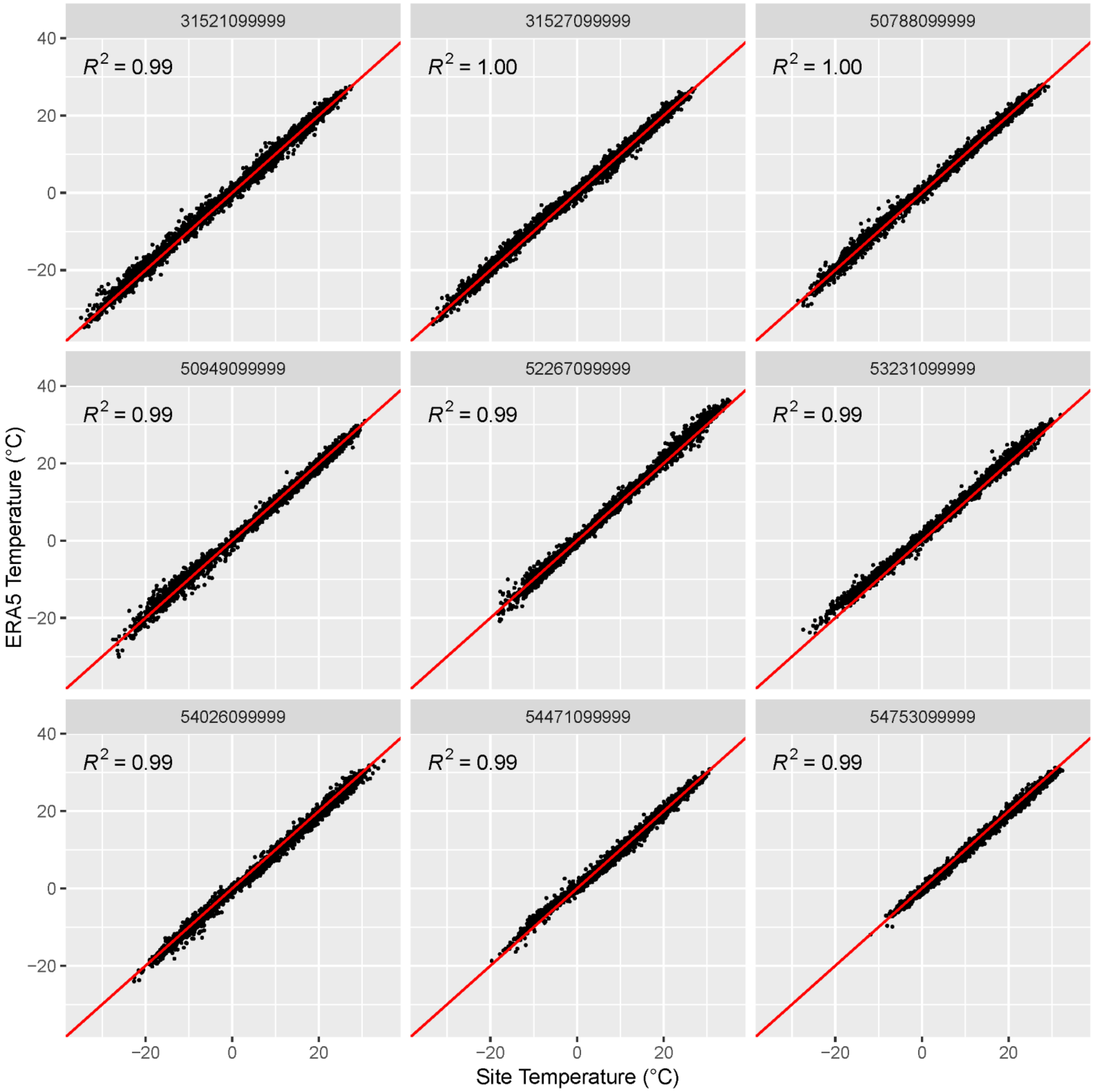

Figure S19. The scatterplot of site and ERA5 temperature (sites with max correlation coefficients)

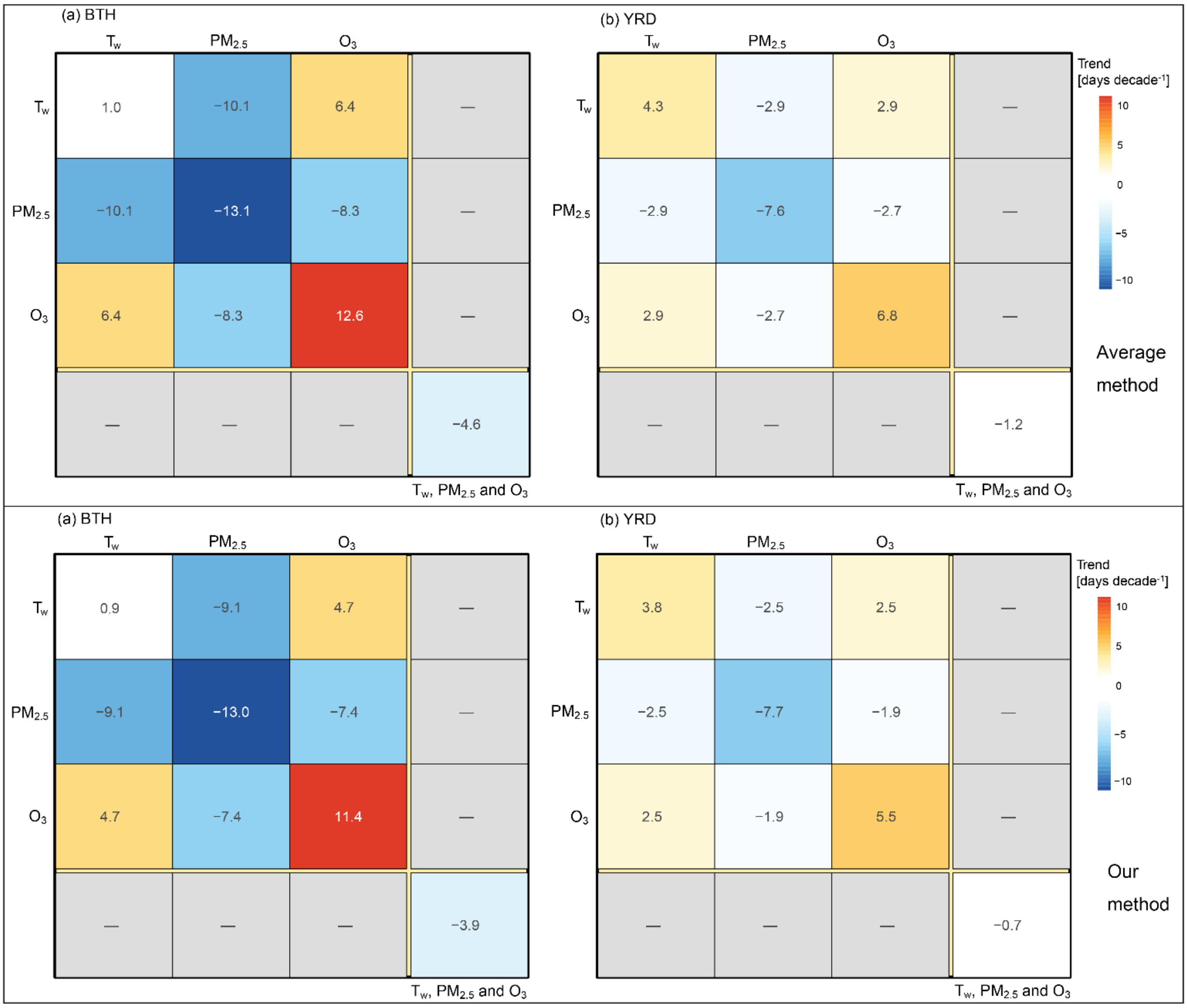

Figure S20. Comparison of results yielded from conventional method and our method

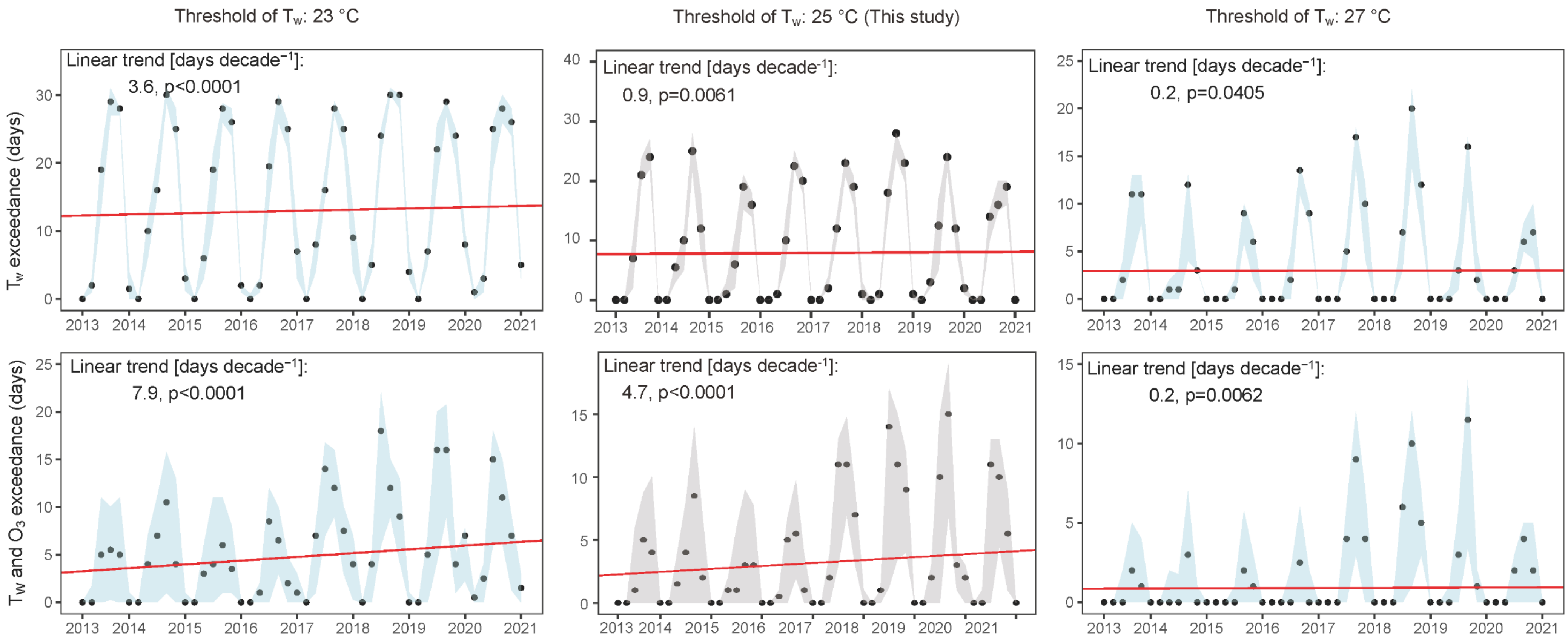

Figure S21. Trend of exceedance days using different threshold values (BTH region).

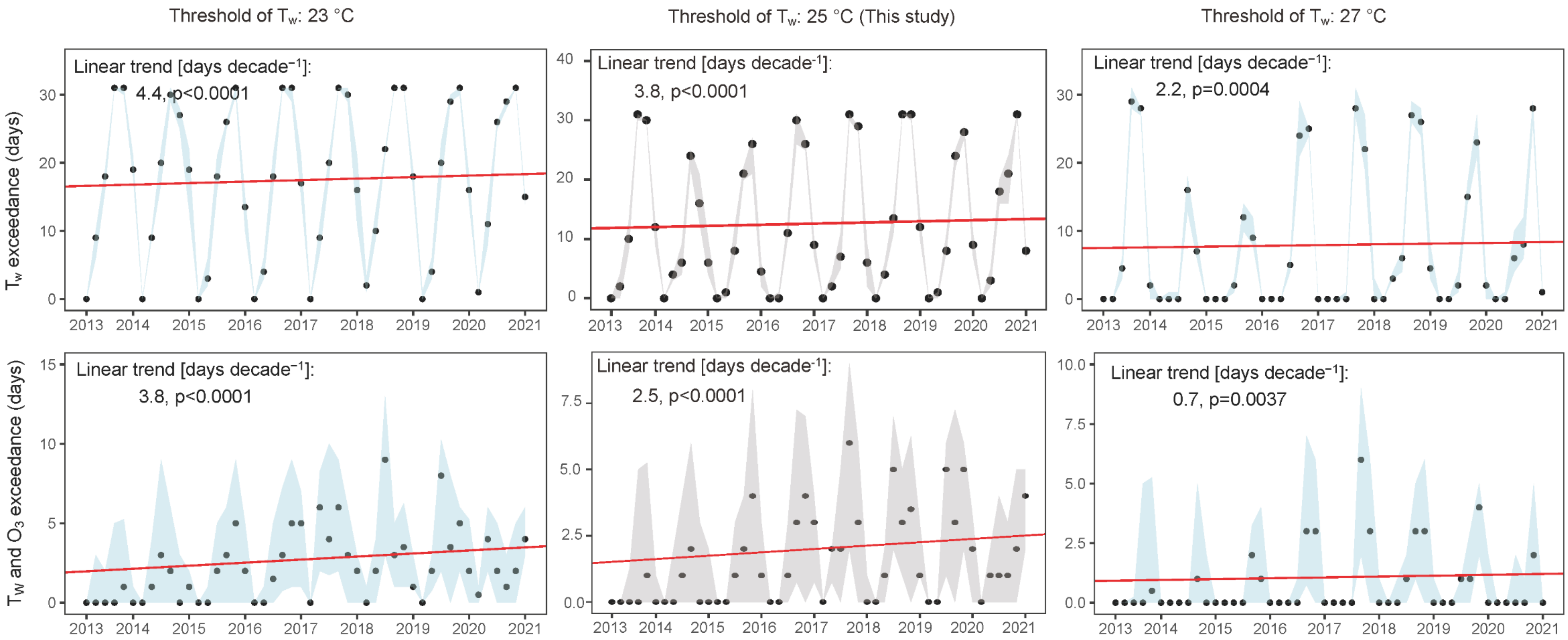

Figure S22. Trend of exceedance days using different threshold values (YRD region).

Supplementary Information of Methods: Pooling method of trends

The statistical analyses in a meta-analysis are guided by a statistical model that must be previously assumed. The main task of the statistical model is to establish the properties of the trend from which the individual trend estimates have been selected. To accomplish the first purpose in a meta-analysis, that is, to calculate an average trend, two statistical models can be assumed: the fixed- and the random-effects models. We used the fixed- effects models for this study.

Suppose there are k independent empirical sites and T_i is the trend estimate obtained in the ith stie. In the fixed-effects model, it is assumed that all of the effect-size estimates in our case, trend estimates, come from a population with a common parametric effect size, θ, and as a consequence the only error source is that produced by sampling error, e_i. Thus, the model can be formulated as $T_i = \theta + e_i$, the sampling errors, e_i, being normally distributed with mean 0 and sampling variance , ei ~ N (0, σ_i^2). Therefore, the effect-size estimates, T_i, are also normally distributed with mean θ and sampling variance σ_i^2, Ti ~ N(θ, σ_i^2).

To calculate an average effect size from a set of studies, each effect-size estimate must be weighted by its precision. In a fixed-effects model, the uniformly minimum variance unbiased estimator (UMVUE) of the average effect size, μ, is that obtained by weighting each effect-size estimate by its inverse variance:

$$T_{UMVUE} = \sum_{i=1}^{k} w_i T_i \Big/ \sum_{i=1}^{k} w_i$$

where w_i is the optimal weight for the ith study and it is defined as $w_i = 1/\sigma_i^2$ in fix-effect models.

Then the combined effect-size (trend) μ, is estimated by:

$$T_{FE} = \sum_{i=1}^{k} \widehat{w}_i T_i \Big/ \sum_{i=1}^{k} \widehat{w}_i$$

T_{FE} is approximately normally distributed and its sampling variance defined as:

$$Var(T_{FE}) = 1 \Big/ \sum_{i=1}^{k} \widehat{w}_i$$

Thus, the confidence interval for the average effect size (trend) can be obtained by:

$$T_{FE} \pm Z_{\alpha/2}\sqrt{Var(T_{FE})}$$

where $Z_{\alpha/2}$ is the 100*(α/2) percentile of the standard normal distribution and α is a significance level. We used α=0.05 in this study, the $Z_{\alpha/2}$ is 1.96 to calculate the 95% confidence interval.